NTNU – Trondheim
Norwegian University of
Science and Technology

Digital Predistortion Linearization of Power Amplifier for X-band Radar System

Magnus Bache

Master of Science in Electronics
Submission date: July 2015
Supervisor: Morten Olavsbråten, IET
Co-supervisor: Asgeir Nysæter, FFI

Norwegian University of Science and Technology
Department of Electronics and Telecommunications

Summary

Modern communication systems with advanced modulation schemes have increased the linearity demands of power amplifiers. This thesis investigates the use of behavioral modeling of power amplifiers to perform digital predistortion on a GaN PA from Cree intended as the transmitter PA in an X-band MIMO-OFDM radar system currently in development by the Norwegian Defence Research Establishment (FFI). Predistortion is a technique where the non-linear distortion of the PA is ideally removed by introducing a unit with the inverse distortion characteristics of the PA. The cascade of the predistorter and the PA thus achieves a linear input/output relationship. By linearizing the PA there is potential for higher power outputs without suffering too much distortion which also leads to an efficiency benefit.

In order to perform digital predistortion linearization, a number of behavioral models based on the Volterra series have been used. Behavioral models are mathematical models describing the relationship between the PA input and output. They require no knowledge about the physical structure of the PA, which is advantageous as this information rarely is available. Three models have been evaluated; the memoryless complex power series (CPS) model, the Wiener model and the memory polynomial (MP) model. The models are implemented in MATLAB and used to describe the behavior of two radio frequency power amplifiers with different operating frequencies, the first being a PA designed at NTNU based on the Cree 10W GaN transistor, and the second being the Cree CMPA5585025F GaN PA intended as the transmitter PA in the radar system. Characterization measurements are performed using a 16-QAM signal and by using the indirect learning architecture, the digital predistortion coefficients are calculated and applied to the input signal. Linearization is then performed on both a 16-QAM signal and an OFDM signal. The results show that the adjacent-channel-power ratio (ACPR) and the error-vector magnitude (EVM) of the 16-QAM signal can be reduced by 15 dB and 5% respectively for the 10W PA at the 1-dB compression point, but only an ACPR reduction of 5 dB was achieved for the OFDM signal. Linearization of the 25W PA only received an ACPR and EVM reduction of 6 dB and 3% respectively for the 16-QAM signal, however the ACPR reduction for the OFDM signal surpassed this, achieving more than 10 dB reduction. The reason for the poorer linearziation performance of the 25W PA was found to be large memory effects leading to less accurate behavioral modeling, even for models incorporating memory. For both of the PAs and signals the linearization performance was quickly reduced as the output power was increased. Thus for higher power outputs, there are less linearization benefits. The results lead to a conclusion that there are not very clear benefits of implementing digital predistortion in the radar system.

Sammendrag

Moderne kommunikasjonssystemer med avanserte modulasjonsteknikker har økt linearitetskravene til effektforsterkere. I denne rapporten brukes matematiske modeller kalt *behavioral models* til å beskrive oppførselen til, og utføre digital predistorsjon på en GaN effektforsterker (PA) fra Cree. PAen er tenkt å brukes på senderutgangen i et X-bånds MIMO-OFDM radarsystem under utvikling av Forsvarets forskningsinstitutt (FFI). Predistorsjon er en lineariseringteknikk hvor den ulineære distorsjonen som innføres av PAen kanselleres av en blokk som har den inverse distorsjonkarakteristikken til PAen. Kaskaden av denne blokken sammen med PAen gir da ideelt sett et lineært forhold mellom inngang og utgang. Linearisering av PAen gir potensial for at utgangseffekten kan økes uten at det innføres for mye distorsjon, noe som også fører med seg effektivitetsfordeler.

For å utføre digital predistorsjon har behavioral modeller basert på Volterra-rekkene blitt brukt. Disse matematiske modellene beskriver forholdet mellom PAens inngangs- og utgangssignaler. De krever således ingen kunnskap om PAens fysiske struktur og oppbygning, noe som er fordelaktig da slik informasjon sjeldent er tilgjengelig. Tre modeller har blitt evaluert; memoryless complex power series-modellen, Wiener-modellen og memory polynomal-modellen. Disse er implementert i MATLAB og deretter brukt til å beskrive oppførselen til to effektforsterkere med forskjellige frekvensområder. Den første er designet ved NTNU og er basert på Crees 10W GaN transistor, og den andre er Crees CMPA5585025F PA tenkt som senderforsterkeren i radarsystemet. Karakteriseringsmålinger er gjort med et 16-QAM-signal og ved å bruke den indirekte læringsarkitekturen, kalkuleres predistorsjonskoeffisientene og påtrykkes inngangssignalet. Linearisereingen er gjort både på et 16-QAM-signal og et OFDM-signal. Resultatene viser at adjacent-channel-power forholdet (ACPR) og error-vector magnitude (EVM) for 16-QAM-signalet kan reduseres med henholdsvis 15 dB of 5% for 10W PAen ved 1-dB kompresjon, men bare en ACPR-reduksjon på 5 dB ble oppnådd på OFDM-signalet. Linearisering af 25W PAen oppnådde bare en ACPR- og EVM-reduksjon på henholdsvis 6 dB og 3% ved 1-dB kompresjon for 16-QAM-signalet, men ACPR-reduksjonen for OFDM-signalet overgikk dette og oppnådde en reduksjon påmer enn 10 dB. Årsaken til 25W PAens dårligere lineariseringsresultater var at den viste store memory-effekter, som igjen førte til en mindre nøyaktig beskrivelse av oppførselen dens med de matematiske modellene, selv for modeller som tar høyde for memory. For begge PAene og signalene ble linearisereingen dårligere når utgangseffekten økte, som betyr at for høyere utgangseffekter mindre å hente ved linearisering. Resultatene førte til en konklusjon om at det ikke er vist veldig klare fordeler ved å implementere digital predistorsjon i radarsystemet.

Preface

This thesis is submitted in partial fulfillment of the degree of Master of Science in the field of electrical engineering at the Norwegian University of Science and Technology (NTNU). The work was conducted in the spring of 2015 under the supervision of associate professor Morten Olavsbråten, and was submitted to NTNU at July 2, 2015. The assignment was given by Asgeir Nysæter at the Norwegian Defence Research Establishment (FFI) as part of a project to develop an experimental X-band MIMO-OFDM radar system.

Acknowledgements

First of all I would like to thank my supervisor at NTNU Morten Olavsbråten. His experience and insight has been truly invaluable during the work on this thesis. I would also like to thank Asgeir Nysæter and Harald Iwe at FFI for giving me the opportunity to work with this project. I would like to give a special thanks to my fellow students Richard Samuelsen, for allowing me to use his power amplifier in my thesis, and Fabian Eckholdt for valuable insight on my work. Finally I would like to thank all the friends I've made here at NTNU for many unforgettable memories during our five years together.

Trondheim, Norway, July 2015

Magnus Bache

Table of Contents

List of Tables

List of Figures

Chapter 1

Introduction

1.1 Motivation

The increased complexity of modern wireless communication systems have increased the performance demand of radio frequency power amplifiers (RFPAs). Modern modulation techniques allowing higher data-rates are more complex and are more vulnerable to distortion due to non-linearities than traditional constant envelope modulation schemes. In addition, modern wideband multi-carrier systems have specific requirements for the power allowed in adjacent channels. This results in more stringent demands of the linearity performance of PAs.

This thesis investigates the use of digital predistortion (DPD) to improve the linearity of the GaN based CMPA5585025F RFPA from Cree. Predistortion is a concept where the input signal is distorted beforehand, through an operation which has the inverse characteristics of the PA, and ideally cancels the distortion from the non-linear PA. The goal is to achieve a linear relationship between the predistorter input, and the PA ouptut. There exist analog predistortion techniques, however they are highly unconfigurable and often require complex circuits and often has lower linearization performance than DPD [1]. With modern high-speed digital circuits, DPD has shown great improvements in PA linearity by reducing figures such as adjacent-channel-power ratio (ACPR) and error-vector magnitude (EVM), and has become the most popular method of PA linearization in the later years [2, 3].

The PA up for linearization is intended as the transmitter PA of an experimental X-band multiple-input-multiple-output orthogonal frequency division multiplexing (MIMO-OFDM) radar system currently in development by the Norwegian Defence Research Establishment (FFI). MIMO-OFDM is a communication scheme capable of achieving high spectral efficiency, and thus high capacity and data rates. It is therefore used as a foundation for many advanced communication standards like WLAN and mobile networks [4]. In a radar

system, MIMO has the advantage of increasing spatial resolution and improves the probability of target detection, and also improves the immunity to interference. Combined with OFDM, frequency selective fading can be reduced. Frequency selective fading can cause dips in the signal-to-noise ratio (SNR), and by introducing frequency diversity through OFDM, this can be reduced [5]. OFDM signals tend to be more vulnerable to the non-linear amplification in the PA than single-carrier systems due to the use of several independent sub-carriers resulting in a pulse with a high peak-to-average power ratio (PAPR). Non-linearities in the PA will reduce modulation fidelity in the desired sub-bands, and cause spectral regrowth [6]. This motivates the need for linearization of the transmitter PA.

Linearizing the transmitter PA has several advantages to the radar system. By reducing the non-linear distortion, it's easier to extract accurate information about the radar target. In addition, assuming there is an upper limit to how much distortion can be tolerated, linearization will allow the PA to be driven harder before reaching this limit. This allows for more output power and also increases power efficiency. The former is important in order to increase the range and probability of radar target detection, and the latter is important in order to reduce the need of cooling.

1.2 Objectives

The main objective of this thesis is to investigate the linearization performance of digital predistortion on Cree's CMPA5585025F Gallium Nitride power amplifier. This is done by using several power amplifier behavioral models based on the Volterra series. This includes the memoryless complex power series, the two-box Wiener and Hammerstein models, and the memory polynomial model. The models are evaluated through their linearization abilities at the cost of computational complexity, and are compared to each other and the theoretical achievable limit. The goal is to achieve high linearization at low computational cost, and without too much increase in the signal's spectral bandwidth. Linearization performance is evaluated on both a 16-QAM and an OFDM signal.

1.3 Report Outline

Chapter 2 explains the background theory and notation used in the report. A basic understanding of the topics are required to understand the work in the report.

Chapter 3 explains the concept of behavioral modeling of power amplifiers and introduces some of these models and how they are derived. These models are used as a basis for the predistortion operation.

Chapter 4 explains the concept of digital predistortion, and how this can be used to linearize a power amplifier through the behavioral models from chapter 3.

Chapter 5 explains the methodology of testing algorithms and performing measurements, both when characterizing the power amplifier and performing predistortion.

Chapter 6 presents the PA behavioral modeling and linearization results obtained through measurements.

Chapter 7 discusses the results from chapter 6 and evaluates the different models' ability to achieve linearization through digital predistortion.

Chapter 8 concludes the report and includes suggestions for further work on this topic.

Chapter 2

Theory

This chapter explains the background theory required to follow the analyses of this report.

2.1 Notation

This section explains the mathematical notation used in this report.

Continuous-time baseband signals are denoted with lowercase font, and with regular parentheses $x(t)$, while the RF passband signals are denoted with a bar $\bar{x}(t)$. Discrete-time signals are denoted with brackets $x[n]$, where n is the time sample index.

Matrices are denoted with uppercase bold font $\mathbf{A}$, column vectors are denoted with lowercase bold font $\mathbf{b}$, and row vectors are denoted as transposed column vectors $\mathbf{b}^T$. Least-squares estimates are denoted with a hat $\hat{\mathbf{b}}$. Matrices consisting of submatrices are denoted in bold font with underline $\underline{\mathbf{A}} = \begin{bmatrix}\mathbf{X_1} \cdots \mathbf{X_N}\end{bmatrix}$.

Matrix conjugate, transpose and conjugate (Hermitian) transpose are denoted $\mathbf{A}^*$, $\mathbf{A}^T$ and $\mathbf{A}^H$ respectively.

2.2 Digital Modulation Techniques

Digital modulation techniques encode the signal information as bits and transfer them over a communication channel. The information bits may come from a digital source or an analog source that has passed trough an A/D-converter. Digital modulation thus consists of mapping the information bits into an analog signal for transmission [7, p.126]. This section briefly explains the two digital modulation techniques which are important

to understand in this thesis; 16-QAM and OFDM. It also explains the power-to-average power ratio (PAPR) and how it's defined in this thesis for the two different modulation techniques.

2.2.1 Quadrature Amplitude Modulation

Quadrature amplitude modulation (QAM) encodes the information bits in both the amplitude and phase of the transmitted signal. This means that QAM can encode more bits per symbol than techniques like phase shift keying (PSK) or pulse amplitude modulation (PAM) which use phase or amplitude alone [7, p.148]. 16-QAM have 16 different symbols in a square constellation and can thus encode $log_2(16) = 4$ bits per symbol. The constellation diagram for a 16-QAM signal with the three amplitude levels is shown in figure 2.1.

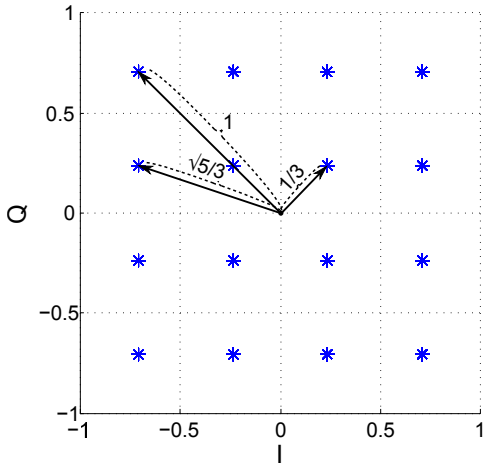

Figure 2.1: Constellation diagram for 16-QAM.

16-QAM is used in this thesis because it's easy to both visually observe and mathematically compute the phase and amplitude distortion introduced by the power amplifier and how predistortion reduces this.

2.2.2 Orthogonal Frequency-Division Multiplexing

Orthogonal frequency-division multiplexing (OFDM) is a digital multi-carrier modulation technique, sending several different bit-streams on different orthogonal sub-channels. The bandwidth of each sub-channel is low, so that it experiences little intersymbol interference (ISI). By introducing what's called a cyclic prefix, ISI can in fact be completely removed for OFDM signals [7]. On each sub-channel the information bits may be encoded using a single-carrier modulation technique like QAM. An OFDM symbol with N sub-carriers can be expressed using the inverse fast Fourier-transform (IFFT) as [7, p.286]:

$$x[n] = \frac{1}{\sqrt{N}} \sum_{i=0}^{N-1} X[i] e^{j2\pi ni/N}, \quad 0 \leq n \leq N-1 \tag{2.1}$$

Figure 2.2 illustrates how an OFDM transmitter is implemented with the IFFT.

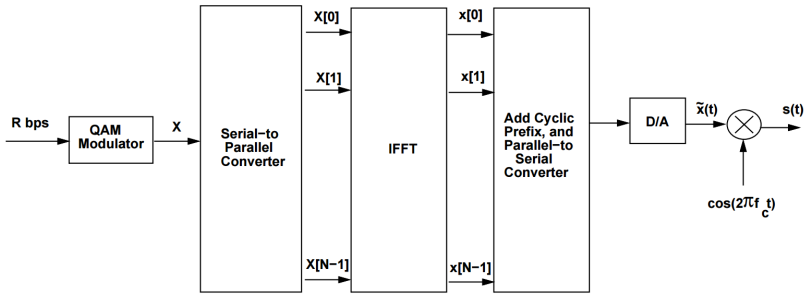

Figure 2.2: OFDM transmitter with IFFT implementation [7].

The orthogonality of the sub-channels allow adjacent channels to be partly overlapping, increasing the spectral efficiency of the signal. This is illustrated in figure 2.3 where the frequency spectrum of an OFDM signal with 8 overlapping sub-carriers is shown.

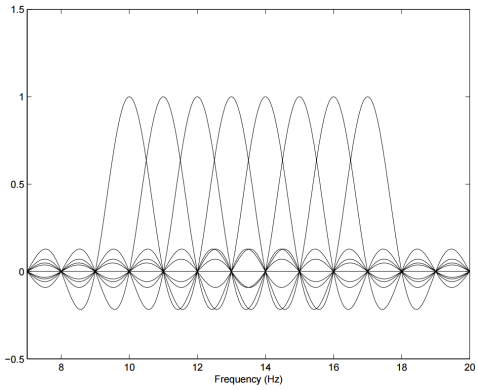

Figure 2.3: Frequency spectrum of an OFDM signal with 8 overlapping sub-carriers [7].

The radar signal is an OFDM signal consisting of 16 sub-carriers spaced 3.125 MHz, giving a total bandwidth of 50 MHz, however the OFDM signal transmitted in this thesis has a bandwidth of 10 MHz due to the signal generator's maximum sampling frequency of 100 MHz [8]. This is elaborated further in section 5.2.3.

2.2.3 The Peak-to-Average Power Ratio

The peak-to-average power ratio (PAPR) of a signal is important to the design of any communication system. Signals with higher PAPR force the transmitter PA to be operated in power back-off in order to ensure linear amplification [7, p.393]. This reduces the maximum power output and efficiency of the PA.

For continuous-time signals, PAPR is defined as [7]:

$$\text{PAPR} = 10log_{10}\left[\frac{max|x(t)|^2}{\mathbf{E}\{|x(t)|^2\}}\right] \tag{2.2}$$

Since the input signal to the PA is analog, this is the definition which gives the most sense to use, however when illustrating PAPR it's easier to use the PAPR definition for discrete-time signals:

$$\text{PAPR} = 10og_{10}\left[\frac{max|x[n]|^2}{\mathbf{E}\{|x[n]|^2\}}\right] \tag{2.3}$$

For a 16-QAM signal with a uniform symbol distribution, the PAPR is:

$$\text{PAPR}_{16QAM} = 10log_{10}\left[\frac{(1)^2}{\frac{4}{16}(1)^2 + \frac{8}{16}(\frac{\sqrt{5}}{3})^2 + \frac{4}{16}(\frac{1}{3})^2}\right] = 2.6 \text{ dB} \tag{2.4}$$

For OFDM signals the PAPR is usually computed in a different manner. Considering the OFDM symbol from equation 2.1:

$$x[n] = \frac{1}{\sqrt{N}}\sum_{i=0}^{N-1} X[i]e^{j2\pi ni/N}, \quad 0 \leq n \leq N-1$$

If the number of sub-carriers N is large, the central limit theorem may be applied, resulting in $x[n]$ being complex zero-mean random variables with Gaussian distribution [7, p.394]. The results in the envelope of the OFDM signal having a Rayleigh distribution with variance σ^2 and a uniform phase. The Rayleigh distribution has infinite support, meaning that the signal envelope peak will exceed any given value with a non-zero probability. As shown in [9], the probability of the PAPR exceeding a threshold $P_0 = \frac{\sigma_0^2}{\sigma^2}$ is given by [7, p.394]:

$$Prob\{\text{PAPR} \geq P_0\} = 1 - (1 - e^{-P_0})^N \tag{2.5}$$

The maximum PAPR for an OFDM signal with N sub-carriers can be computed by looking at N Gaussian independent and identically distributed complex random variables x_n ($0 \leq$

$n \leq N-1$) with zero mean and unit power. With equation 2.1 as a basis, the average power of the signal is given by [7, p.394]:

$$\mathbf{E}\{|x[n]|^2\} = \frac{1}{N}\mathbf{E}\{|x_0 + \cdots + x_{N-1}|^2\}$$

$$= \frac{1}{N}\Big[\mathbf{E}\{|x_0|^2\} + \cdots + \mathbf{E}\{|x_{N-1}|^2\}\Big] = 1 \tag{2.6}$$

The maximum PAPR value occurs when all x_i add coherently:

$$max|x[n]|^2 = \left|\frac{N}{\sqrt{N}}\right|^2 = N \tag{2.7}$$

Thus the maximum PAPR is equal to the number of sub-carriers N. The probability of this occurrence becomes lower as N increases. The OFDM signal used in this thesis consists of 16 sub-carriers modulated with BPSK, resulting in a theoretical maximum PAPR of $10log_{10}(16) = 12$ dB, however the probability of this occurring is $1/2^{16}$, i.e. it's highly improbable.

A common way to denote the maximum PAPR of an OFDM signal is by expressing the probability of which it will occur. This is illustrated in figure 2.4, where the fitted probability density function and the corresponding cumulative distribution function of the OFDM signal envelope is plotted, for 10000 different OFDM symbols with 16 carriers.

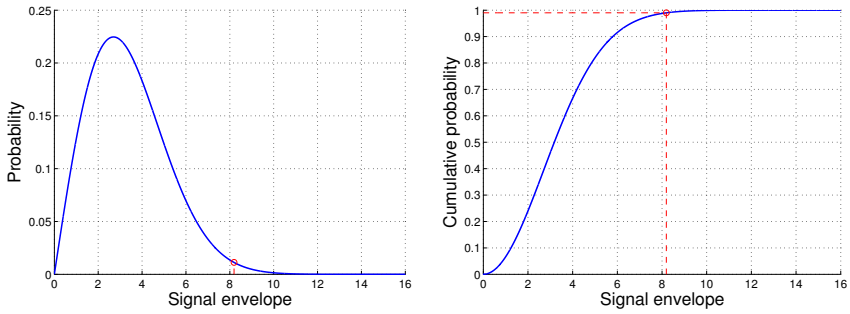

(a) Envelope distribution. **(b)** Cumulative distribution.

Figure 2.4: OFDM signal envelope distribution.

The PAPR of the OFDM signal covering 99% of the outcomes, denoted $\text{PAPR}_{99\%}$, is seen from the red dotted line in figure 2.4:

$$\text{PAPR}_{99\%} = 8.2 = 9.1 \text{ dB} \tag{2.8}$$

In communication systems, signals pass through a pulse shaping filter in order to reduce sidelobe energy which may cause adjacent channel interference, and reduce ISI. This will

increase the PAPR of the signal by preserving the peak values, but lowering the average power. Thus, the PAPR of the analog input signal to the PA will in fact be higher than the theoretical non-filtered values computed in this section. The actual PAPR of the two different input signals is specified in chapter 5.

2.3 Least-Squares Minimization

In order to perform digital predistortion as explained in this thesis, it becomes necessary to solve sets of linear equations to estimate the optimal DPD coefficients. This can be done through least-squares minimization. A least-squares problem is an optimization problem with an objective which is a sum of squares of terms on the form $\mathbf{a}_i^T\mathbf{x} - \mathbf{b}_i$, and with no constraints. The convex optimization problem of least-squares minimization can be formulated as [10, p.4]:

$$\text{minimize } \|\mathbf{A}\mathbf{x} - \mathbf{b}\|_2^2 = \sum_{i=0}^{N-1} (\mathbf{a}_i^T\mathbf{x} - \mathbf{b}_i)^2 \tag{2.9}$$

Where $\mathbf{A} \in \mathbb{C}^{N\times M}$, $\mathbf{a}_i^T$ are the rows of $\mathbf{A}$, $\mathbf{b} \in \mathbb{C}^N$ and $\mathbf{x} \in \mathbb{C}^M$ is the optimization variable. An RFPA is usually an overdetermined system, meaning there are more equations than unknowns in the system, i.e. $N > M$. The solution of the least-squares problem in 2.9 can be found by solving a set of linear equations:

$$(\mathbf{A}^H\mathbf{A})\mathbf{x} = \mathbf{A}^H\mathbf{b} \tag{2.10}$$

The goal of the optimization problem is thus to find the vector $\hat{\mathbf{x}}$ which minimizes the residual of the Euclidean norm $\|\cdot\|_2$ of $\mathbf{A}\mathbf{x} - \mathbf{b}$:

$$\hat{\mathbf{x}} = (\mathbf{A}^H\mathbf{A})^{-1}\mathbf{A}^H\mathbf{b} \tag{2.11}$$

In order to solve 2.11 matrix $\mathbf{A}$ needs to have full rank. A matrix $\mathbf{A} \in \mathbb{C}^{N\times M}$ has full rank if $rank\{\mathbf{A}\} = min\{N, M\}$ [10, p.646], meaning $\mathbf{A}$ must contain M linearly independent rows. In order to solve 2.11 in the case of rank deficiency, singular value decomposition is used to find the pseudo-inverse, or Moore-Penrose inverse of matrix $\mathbf{A}$.

A matrix $\mathbf{A} \in \mathbb{C}^{N\times M}$ with $rank\{\mathbf{A}\} = R$ can be factored as [10, p.649]:

$$\mathbf{A} = \mathbf{U}\mathbf{\Sigma}\mathbf{V}^H \tag{2.12}$$

Where $\mathbf{U} \in \mathbb{C}^{N\times R}$ satisfies $\mathbf{U}^H\mathbf{U} = \mathbf{I}$, $\mathbf{V} \in \mathbb{C}^{R\times M}$ satisfies $\mathbf{V}^H\mathbf{V} = \mathbf{I}$, and $\mathbf{\Sigma} = diag(\sigma_1, \cdots, \sigma_r)$, with $\sigma_1 \geq \sigma_2 \geq \cdots \geq \sigma_r > 0$

The pseudo-inverse of matrix $\mathbf{A}$ is defined as:

$$\mathbf{A}^{\dagger} = \mathbf{V}\mathbf{\Sigma}^{-1}\mathbf{U}^{H} \tag{2.13}$$

In the case of solving the least-squares problem when the solution is not unique, $\mathbf{A}^{\dagger}\mathbf{b}$ gives the solution with the minimum Euclidean norm.

A more detailed derivation of the pseudo-inverse and its applications can be found in [10, p.649].

In this thesis, the least-squares approach to minimzation is used to estimate the optimal coefficients of the DPD operation.

2.4 Effects of Non-linearity in Power Amplifiers

This section describes some of the effects occurring due to non-linearity in power amplifiers. Through knowledge how these effects behave, their corrupting impact on the output signal of the PA can be reduced by using digital predistortion.

2.4.1 AM/AM Distortion

AM/AM distortion, or gain compression in power amplifiers comes from the fact that the active components in the system are non-linear. To understand this phenomenon it's necessary to take a look at the non-linear model describing the output signal from a non-linear system. From [11, p.14], the input/output characteristic of a memory-less system can be expressed as

$$y(t) = \alpha_1 x(t) + \alpha_2 x^2(t) + \alpha_3 x^3(t) + \cdots \tag{2.14}$$

where $y(t)$ is the output and $x(t)$ is the input of the system. To simplify analysis, only the first three terms of 2.14 are included. Assuming $x(t)$ is a sinusoidal signal of amplitude A and angular frequency ω:

$$x(t) = Acos\omega t \tag{2.15}$$

Inserted in 2.14 this gives:

$$y(t) \approx \alpha_1 Acos\omega t + \alpha_2 A^2 cos^2\omega t + \alpha_3 A^3 cos^3\omega t \tag{2.16}$$

$$= \alpha_1 Acos\omega t + \frac{\alpha_2 A^2}{2}(1 + cos2\omega t) + \frac{\alpha_3 A^3}{4}(3cos\omega t + cos3\omega t) \tag{2.17}$$

$$= \frac{\alpha_2 A^2}{2} + (\alpha_1 A + \frac{3\alpha_3 A^3}{4})cos\omega t + \frac{\alpha_2 A^2}{2}cos2\omega t + \frac{\alpha_3 A^3}{4}cos3\omega t \tag{2.18}$$

The second term of 2.18 is the fundamental. The voltage gain experienced by $x(t)$ is thus given by

$$G_V = \frac{(\alpha_1 A + \frac{3\alpha_3 A^3}{4})cos\omega t}{Acos\omega t} = \alpha_1 + \frac{3\alpha_3 A^2}{4} \tag{2.19}$$

From 2.19 it's clear that the gain is affected not only by α_1, but also by α_3 and A. Further it's important to note that for most RF circuits $\alpha_1\alpha_3 < 0$, which leads to a compressive behaviour. This means that the gain decreases as A increases, causing compression of the fundamental voltage gain.

A common measure used to describe this effect is the 1-dB compression point. This is the point where the actual gain experienced by the fundamental component is 1 dB below the small signal voltage gain α_1. A is the amplitude of the input signal $x(t)$. The 1-dB compression point related to the system's input amplitude can be expressed as:

$$20log_{10}\left|\alpha_1 + \frac{3\alpha_3 A_{in,1dB}^2}{4}\right| = 20log_{10}|\alpha_1| - 1 \text{ dB} \tag{2.20}$$

$$A_{in,1dB} = \sqrt{0.145\frac{|\alpha_1|}{|\alpha_3|}} \tag{2.21}$$

An illustration of the 1-dB compression point is shown in figure 2.5 where output versus input power is plotted for an ideal and a compressive amplifier.

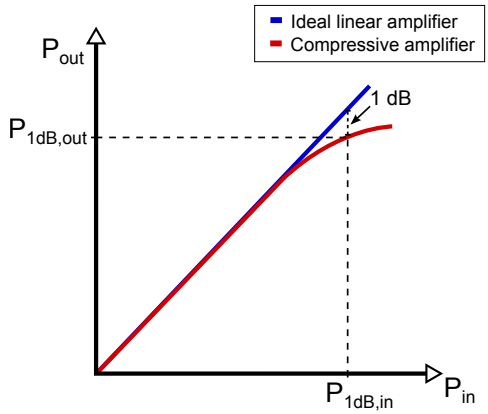

Figure 2.5: Illustration of 1-dB compression point for a power amplifier

For signals with high PAPR, the high power peaks will suffer from large amounts of gain compression. To achieve linear operation, the input power needs to be reduced, limiting both the output power and the power efficiency of the PA. Through digital predistortion linearization AM/AM distortion can be reduced, allowing higher output power without suffering from too much distortion, and higher efficiency.

2.4.2 AM/PM Distortion

In addition to causing compression of the output signal amplitude, the input signal amplitude may be converted to a phase shift at the PA output, producing what is called AM/PM distortion. This effect can in general be traced to the signal-dependency of key transistor elements. For FETs, the input capacitance and the depletion and junction resistance of the gate-source diodes may cause AM/PM distortion [2, p.252].

Considering a PA input signal $v_i(t) = A_1 cos\omega t$. For a PA with AM/PM distortion, the fundamental output component is given by [11, p.33]:

$$v_o(t) = A_2 cos\big[\omega t + \phi(A_1)\big] \tag{2.22}$$

where $\phi(A_1)$ is the amplitude-dependent phase shift. As explained in [2, p.253], the most significant effect of this phase shift is to generate additional terms at the same frequencies as the odd order intermodulation products from AM/AM distortion.

Thus, when AM/PM distortion occurs, variations in the PA's input signal's amplitude will corrupt, or distort, the phase of the output signal causing spectral regrowth.

2.4.3 Memory Effects

"Memory effects" is a term used to describe effects which cause dynamic deviation in the static input/output characteristic of a PA. A circuit can only be truly memoryless if there exists no elements storing electrical charge or magnetic flux [12]. This means the circuit cannot contain any inductors or capacitors, for which the currents and voltages depend on past values of currents and voltages. Thus, all microwave networks must be classified as having memory. [2, p.256] explains how memory effects can be traced to three main causes:

- Dynamic thermal effects
- Modulation of bias circuitry
- Semiconductor trapping effects

Thermal Effects

When the PA is driven at high power the transistor will self-heat, altering its characteristics. This heat will remain high for a period of time, even after power is reduced, resulting in memory in the system. However, the question is whether heat moves around quickly enough to cause non-linear changes on an observable timescale. Steve Cripps states in [2, p.258] that when the timescale is measured in a signal modulation domain from tens of nanoseconds up to milliseconds, thermal memory effects may cause about 0.1 dB of gain variation for most varieties of RF semiconductor technologies. This timescale covers the time domain of typical communication signals and will thus cause dynamic gain variation.

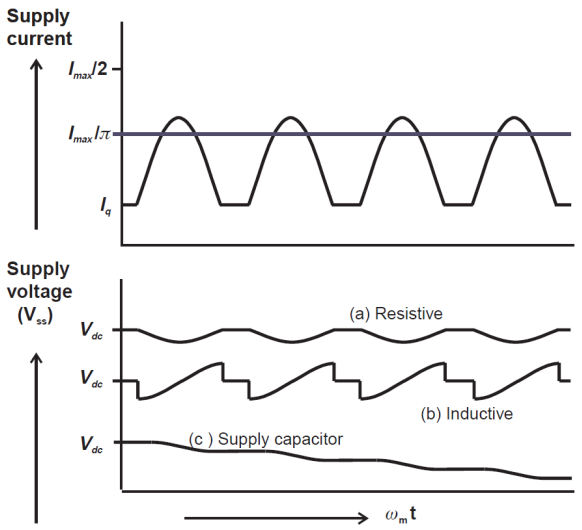

Figure 2.6: Bias supply modulation: a) resistive, b) inductive, c) capacitive [2, p.345].

Modulation of Bias Circuitry

Any impedance in the bias supply path will cause a voltage modulation to occur on the output terminal of the transistor. This results in a modulation of the gain and phase of the output signal, resulting in distortion of the signal. The impact of this effect naturally varies with the frequency of the envelope of the modulated signal, and is usually the most common cause of asymmetrical intermodulation sidebands [2, p.256]. Figure 2.6 shows how a resistive, inductive and capacitive series impedance affects the bias supply voltage for a deep Class AB RFPA, at a given angular envelope frequency ω_m.

From figure 2.6 it's clear that ripple in the supply voltage occurs in the same frequency range as the signal envelope. Altering the bias conditions of the transistor, will alter the characteristics of the PA, causing dynamic gain and phase distortion to appear at the PA output as the signal amplitude varies. The question of how much supply ripple can be tolerated, depends entirely on the application and the device technology. Different transistor types show variation in bias sensitivity, and the effects caused by ripple in the bias.

Trapping Effects

Semiconductor trapping effects are according to Cripps in [2, p.256] a generic term which can be used to describe a number of anomalous effects occuring in a semiconductor. Modern gallium nitride (GaN) HEMT devices, such as the one used in this thesis, have traditionally shown more of these trapping effects than other technologies. They occur due to imperfections in the semiconductor structure, such as parasitic atoms and uneven transitions between layers [12]. This may cause passing electrons to be trapped for an unknown

amount of time, before being released, causing a so called "current collapse". This is a temporary reduction in drain current after the application of a high gate voltage level [13]. The release of these electrons is hard to describe as it does not behave deterministically, and is thus hard to account for.

2.5 Basic Microwave Network Analysis

This section explains the basics of performing analysis on microwave networks.

2.5.1 The S-parameters

The scattering parameters, or S-parameters, describe the electrical behaviour of a microwave network by expressing the incident and reflected voltage waves at the different ports of the network [14, p.50]. Figure 2.7 illustrates the incident and reflected waves of a 2-port microwave network.

Figure 2.7: Incident and reflected current and voltage waves for a 2-port microwave network.

The total voltage and current at port i is:

$$V_i = V_i^+ + V_i^- \tag{2.23}$$

$$I_i = I_i^+ - I_i^- \tag{2.24}$$

For the network in figure 2.7, the two dimensional scattering matrix is given by:

$$\begin{bmatrix} V_1^- \\ V_2^- \end{bmatrix} = \begin{bmatrix} S_{11} & S_{12} \\ S_{21} & S_{22} \end{bmatrix} \begin{bmatrix} V_1^+ \\ V_2^+ \end{bmatrix}$$

S_{ij} thus describes the amplitude of the voltage wave V_i^- coming from port i, when port j is driven by a voltage wave of amplitude V_j^+, and all other incident voltage waves are zero.

$$S_{ij} = \left. \frac{V_i^-}{V_j^+} \right|_{V_k^+ = 0 \text{ for } k \neq j} \tag{2.25}$$

For a two-port network, S_{11} and S_{22} describe the reflected incident power at each port, and S_{21} and S_{12} are parameters describing the transmitted power between the two ports. In this thesis, a vector network analyzer is used to measure the magnitude and phase of S_{21} as a function of input power to characterize the PA's non-linear behavior.

2.5.2 The Vector Network Analyzer

A network analyzer is an instrument used for measuring the scattering parameters of a microwave network. A vector network analyzer (VNA), which is the kind used for measurements in this report, measures both magnitude and phase properties of the S-parameters for a device-under-test (DUT). The setup for network analysis of a two-port network can be seen in figure 2.8.

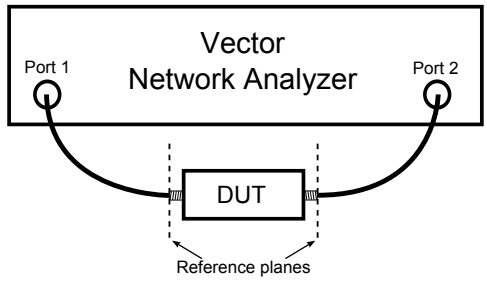

Figure 2.8: Setup for analysis of two-port network using a network analyzer.

To correct for systematic errors in the instrument, characteristics of cables and test fixtures the network analyzer needs to be calibrated to a reference plane. This plane can be placed wherever is desired in a cascade of components which is practical as an attenuator is often needed at the PA output to protect the instrument from high power levels.

For the instrument used for measurements in this report, calibration is done using the *SOLT*-method. SOLT is an acronym for short, open, load, thru. Calibration is performed by connecting each of the ports of the VNA to a standardized calibration kit with a short circuit, open circuit, a 50Ω load and a through connection. After measurements are performed on each of the calibration standard components, correction parameters are calculated by the VNA, and applied to the data. Error calibration is crucial to obtain correct measurement data for the S-parameters.

2.6 Efficiency Analysis of Power Amplifiers

Although the scope of this thesis is not to perform a thorough analysis of the efficiency enhancement possible through predistortion linearization, this issue is still commented throughout the report, which qualifies for some theoretical background.

Power amplifiers are usually the single most power dissipating units in communication systems, and thus their power efficiency is an important factor in PA design. PA efficiency is usually defined by two metrics. The first is called the *drain efficiency* for FETs (or *collector efficiency* for BJTs) and is defined as [11, p.755]:

$$\eta = \frac{P_L}{P_{supp}} \tag{2.26}$$

where P_L is the average power delivered to the load, and P_{supp} is the average power drawn from the power supply. This metric however, does not account for the input power, which often can be high, especially for PAs with low power gain. The second metric, called the *power-added efficiency* (PAE), accounts for this and is defined as:

$$PAE = \frac{P_L - P_{in}}{P_{supp}} \tag{2.27}$$

where P_{in} is the average input power of the PA.

The efficiency of PAs increase as the average output power increases, seen in figure 2.9 where gain and drain efficiency η is plotted for the CGH40010F GaN transistor from Cree. By linearizing a PA with predistortion, it can be driven harder before reaching the same amounts of non-linearities, thus improving both the power output and the efficiency.

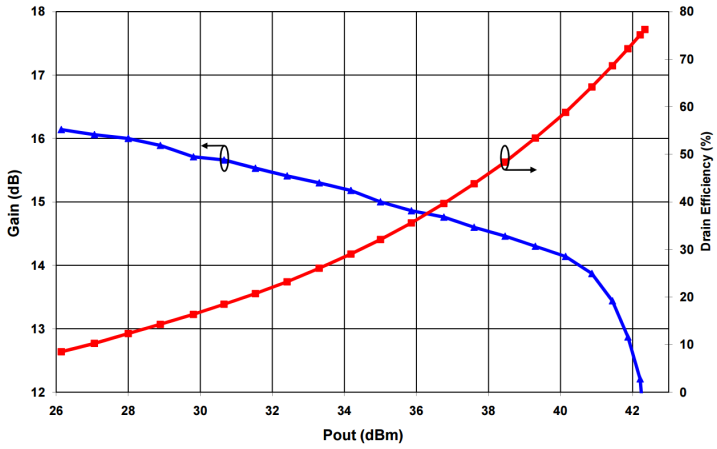

Figure 2.9: Gain (blue) and drain efficiency (red), swept CW Data of CGH40010F vs. Output Power with Source and Load Impedances Optimized for Drain Efficiency at 2.0 GHz $V_{DD} = 28$ V, $I_{DQ} = 200$ mA [15, p.4]

2.7 Predistortion

2.7.1 Introduction to Predistortion

The principle of predistortion is to ideally non-linearities introduced by the PA explained in section 2.4. This is illustrated in figure 2.10.

In [2], the predistortion operation is expressed mathematically by using a simple third-order model for the PAs input/output characteristic:

$$v_o = a_1 v_p + a_3 v_p^3 \tag{2.28}$$

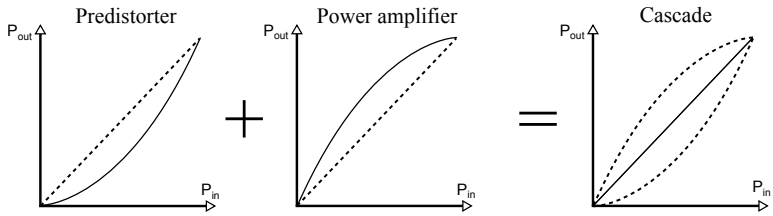

Figure 2.10: Illustration of predistortion.

where the PA input voltage v_p is the output voltage of a predistorter with characteristics

$$v_p = b_1 v_i + b_3 v_i^3 \tag{2.29}$$

The PA output can then be expanded to be:

$$v_o = a_1 b_1 v_i + (a_1 b_3 + a_3 b_1) v_i^3 + 3 a_3 b_1^2 b_2 v_i^5 + 3 a_3 b_3^2 b_1 v_i^7 + a_3 b_3^3 v_i^9 \tag{2.30}$$

In order to cancel the third-order distortion introduced by the second term of equation 2.30, the predistorter can be designed in such a way that:

$$b_3 = -\frac{a_3 b_1}{a_1}$$

This will in fact remove third-order distortion altogether, however it's clear from equation 2.30 that higher order harmonics will not be canceled. This means that the predistorter itself will introduce intermodulation distortion which is not present without predistortion.

Equation 2.29 reveals that the predistorted signal contains higher order harmonics of the input signal, and thus has a significantly larger bandwidth than the original signal. [2, p.402]. This becomes one of the major limitations of predistortion for the radar system. First of all this requires that the sampling rate of the DSP unit is fast enough to produce the predistorted signal without aliasing. For systems with large bandwidth this can be a major constraint in predistorter performance as large bandwidth DACs are usually expensive and have high power consumptions [16]. In addition the analog electronics must have a large enough bandwidth to pass the predistorted signal, and this is a very important consideration which is critical during the radar system design.

2.7.2 Digital Predistortion

Digital predistortion (DPD) has lately become the most active area for PA linearization due to the development of high-speed DSP technology. In order for a system to allow digital predistortion digital baseband information about the amplitude and phase of the PAs input signal is required. This information is only available in a complete transmitter system where the signal is generated from scratch [2]. Figure 2.11 shows a flow chart of a basic DPD PA system.

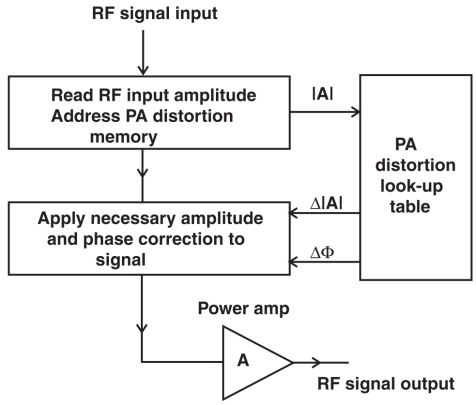

Figure 2.11: Flow chart of basic DPD PA system [2].

Assuming the PA has a quasi-static behaviour, the output voltage has a fixed, monotonic relationship to the input voltage:

$$V_o = F\{V_i(t)\} \tag{2.31}$$

where V_o and V_i are the magnitudes of the output and input RF carrier at the same instant in envelope domain time τ. By characterizing this relationship, a look-up-table (LUT) shown in figure 2.11 can be created using a priori measurements on the PA.

The system shown in figure 2.11 has some obvious limitations. Changes in PA characteristics will reduce the performance of the predistortion process. However, even with adaptive calibration of the LUT, implementations have shown mediocre results [2, p.405]. The fundamental reason for this is the memory effects explained in section 2.4.3 causing short-time variations in PA characteristics. For DPD, there exist models for describing and somewhat compensating for memory effects by including past samples of the input signal, which have shown improvement compared to memoryless models.

It's important to note, however, that the use of a look-up-table for predistortion has major bandwidth drawbacks. The predistorted signal from a LUT will in essence have an infinite bandwidth, which is impossible to achieve digitally due to a finite sampling rate. This will result in aliasing of the spectrum, and will create additional distortion, the severity of which will increase with an increase in signal bandwidth. Instead of using a LUT for predistortion, mathematical behavioral models of finite non-linear order are used in this thesis. These behavioral PA models and their basic derivations are presented in chapter 3. A more detailed explanation of digital predistortion and the PA linearization problem is presented in chapter 4.

Chapter 3

Behavioral Modeling of Power Amplifiers

Power amplifiers are important for the reliability of wireless communication systems and a countless amount of studies have been undertaken to understand their limitations and optimize their performance [17]. PA modeling has been an important field of study in order to allow PAs to be pushed to their limits of operation. By accurately modeling the PA's behavior, an inverse characteristic can be found to perform predistortion. PA modeling is usually divided into two categories according to the type of data needed to extract the model parameters: physical models and empirical models.

Physical models require knowledge of the physical effects occurring in the electronic elements of the PA. These models require a detailed description of the PAs internal structure and such information is usually not available. Behavioral models are on the other hand solely based on input/output observation of the PA. They are thus very sensitive to the model structure and parameter extraction procedure, but are much more efficient in system-level simulations and requires no physical knowledge of the PA. This chapter presents the basics of power amplifier modeling and the behavioral models used for predistortion in this thesis.

3.1 Power Amplifier Modeling Basics

Assuming the PA has a static behavior, it's discrete-time output $y[n]$ can be defined as a non-linear function f of the instantaneous discrete-time input $x[n]$ [17]:

$$y[n] = f\{x[n]\} \tag{3.1}$$

If the PA has memory effects such as those explained in section 2.4.3, it is said to be dynamic. This means that the PA's output can no longer be determined from the instantaneous input, but now also depends on previous input samples. The relation between $y[n]$ and $x[n]$ now becomes a non-linear operator f_D, mapping $x[n]$ to $y[n]$. This relation can be expressed as:

$$y[n] = f_D\Big\{x[n], x[n-1], \cdots, x[n-M]\Big\} \tag{3.2}$$

Operator f_D is a non-linear extension of finite impulse response digital filters and depends on M previous samples of input signal $x[n]$ [17].

Memory effects introduce both linear and non-linear dependencies on previous samples of the input signal, referred to as linear and non-linear memory. The linear memory effects are caused by a non-ideal frequency response at the fundamental frequency, whereas non-linear memory effects come from trapping, matching at harmonic frequencies and poor bias circuit design [18]. As explained in [17], several authors have shown that these effects can be represented as a PA on the form shown in figure 3.1.

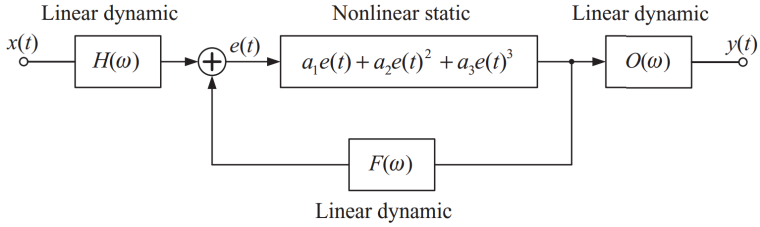

Figure 3.1: Typical non-linear feedback structure of an RFPA [17].

The filters $H(\omega)$ and $O(\omega)$ represent linear memory effects due to input and output matching networks, and $F(\omega)$ represents non-linear memory due to thermal hysteresis, trapping and bias circuitry modulation. The different models presented in the next section have different abilities in representing memory effects.

3.2 Behavioral Models

3.2.1 Volterra Series Model

For a memoryless system, the non-linear input/output characteristics may be described by the Taylor series model:

$$\bar{y}(t) = \sum_{k=1}^{\infty} \bar{c}_k \bar{x}^k(t) \tag{3.3}$$

Where $\bar{x}(t)$ and $\bar{y}(t)$ are the bandpass input and output signals of the system, and $\bar{c}_k$ are constant complex coefficients..

The Volterra series model is a generalization of the Taylor series model, incorporating memory effects. If a system is linear, the continuous-time output $\bar{y}(t)$ can be described by a convolution between the input $\bar{x}(t)$ and the system's impulse response $h(t)$ [12]:

$$\bar{y}(t) = \int_0^\infty \bar{x}(t)h(t-\tau) \tag{3.4}$$

In the linear case 3.4 accurately represents the memory effects of the system. However, in a non-linear system, $\bar{y}(t)$ depends on higher order terms of $\bar{x}(t)$. Thus, a generalization of equation 3.3 is achieved through combination with 3.4, resulting in a series of non-linear integrals representing the output's dependency on all orders of the input [12]:

$$\bar{y}(t) = h_0 + \sum_{k=1}^{\infty} \int_{\tau_1} \cdots \int_{\tau_k} h_k(t, \tau_1, \cdots, \tau_k)\bar{x}(\tau_1)\cdots\bar{x}(\tau_k)d\tau_1\cdots d\tau_k \tag{3.5}$$

where h_0 is the constant zero order kernel, and $h_k(\tau_1, \cdots, \tau_k) = h_k(\tau_1)\cdots h_k(\tau_k)$ are the Volterra kernels.

Due to high computational complexity, the Volterra series behavioral model has not been implemented in this thesis, but is the basis for the other simplified models presented.

3.2.2 Complex Power Series Model

The complex power series is a basic memoryless system-level model. For memoryless models it's assumed that the output envelope reacts instantaneously to changes in the input envelope, and thus assume static AM/AM and AM/PM characteristics. The complex power series model is derived by making the memoryless assumption to the Volterra series in equation 3.5, resolving the kernels into multiple Dirac delta functions [17, p.100]:

$$h_k(\tau_1, \cdots, \tau_k) = \bar{c}_k\delta(t-\tau_1)\cdots\delta(t-\tau_k) \tag{3.6}$$

where $\bar{c}_k$ are constant complex coefficients. This reduces 3.5 to the Taylor series in equation 3.3. Truncating 3.3 to maximum non-linear order K yields:

$$\bar{y}(t) = \sum_{k=1}^{K} \bar{c}_k\bar{x}^k(t) \tag{3.7}$$

where $\bar{x}(t)$ and $\bar{y}(t)$ are the bandpass input and output signals respectively, and $\bar{c}_k$ are constant complex coefficients. The real valued bandpass signal $\bar{x}(t)$ is given by:

$$\bar{x}(t) = Re\{x(t)e^{j2\pi f_c}\} \tag{3.8}$$

where $x(t)$ is the complex baseband signal, and f_c is the RF carrier frequency. As the signal is being generated in baseband, it's desirable to express equation 3.7 from the baseband signal $x(t)$. As explained in [19], the baseband representation is given by:

$$y(t) = \sum_{k=1}^{K} c_k x(t)|x(t)|^{k-1} \tag{3.9}$$

where $x(t)$ and $y(t)$ are the baseband input and output signals respectively, and c_k are the baseband complex coefficients. In discrete-time this becomes:

$$y[n] = \sum_{k=1}^{K} c_k x[n]|x[n]|^{k-1} \tag{3.10}$$

Equation 3.10 can be expressed in matrix form as $\mathbf{y} = \mathbf{Hc} \in \mathbb{C}^N$, where $\mathbf{c} = [c_1, c_2, \cdots, c_K]^T \in \mathbb{C}^{\kappa_{CPS}}$ are the complex coefficients of the model and $\kappa_{CPS} = K$ is the total number of coefficients of the model. $\mathbf{H} \in \mathbb{C}^{N \times K}$ is the regression matrix of the model constructed from the system input signal $x[n]$. For the complex power series it can be written as:

$$\mathbf{H} = \begin{bmatrix} x_0|x_0|^0 & x_0|x_0|^1 & \cdots & x_0|x_0|^{K-1} \\ x_1|x_1|^0 & x_1|x_1|^1 & \cdots & x_1|x_1|^{K-1} \\ \vdots & \vdots & \ddots & \vdots \\ x_{N-1}|x_{N-1}|^0 & x_{N-1}|x_{N-1}|^1 & \cdots & x_{N-1}|x_{N-1}|^{K-1} \end{bmatrix} \tag{3.11}$$

where $\mathbf{x} = [x_0, x_1, \cdots, x_{N-1}]^T$ is the input vector of N samples where $x_n = x[n]$.

To reduce the number of coefficients necessary, and thus computational complexity, many researchers use a model including only odd-orders, which assumes that the PA non-linearities are mostly constructed from odd-order functions[1]. This is implemented to investigate if the number of coefficients may be reduced by using odd-orders only, without losing too much linearization performance.

Estimation of coefficients

The coefficients $\mathbf{c} \in \mathbb{C}^K$ can be estimated through the least-squares method described in section 2.3. This yields:

$$\hat{\mathbf{c}} = (\mathbf{H}^H\mathbf{H})^{-1}\mathbf{H}^H\mathbf{y} \tag{3.12}$$

where $\mathbf{y} = [y_0, y_1, \cdots, y_{N-1}]^T$ is the output vector from the PA corresponding to input $\mathbf{x}$. Thus the baseband model output $\hat{\mathbf{y}}$ can be found:

$$\hat{\mathbf{y}} = \mathbf{H}\hat{\mathbf{c}} \tag{3.13}$$

[1]The modeling results in this thesis show that it's beneficial to also include even-order terms for the PAs in question. This is also seen in [12, 20]

3.2.3 Two-box Models

Two-box models are subsets of the Volterra series and are obtained by modeling the system as a combination of a static, memoryless non-linearity and a linear, time-invariant dynamic subsystem [17], and are capable only of representing linear memory effects. For the implementation used in this report, the static non-linearity is represented by the baseband complex power series polynomial $x[n]|x[n]|^{k-1}$. The dynamic LTI-system is a FIR filter of order M. These two subsystems may be arranged in either way, producing the Wiener and Hammerstein models shown in figures 3.2 and 3.3.

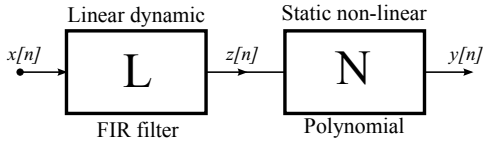

Figure 3.2: The two-box Wiener model [17, p.137].

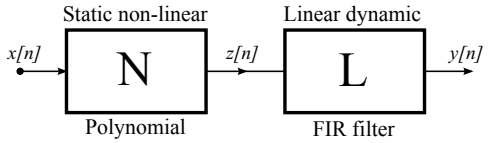

Figure 3.3: The two-box Hammerstein model [17, p.137].

Estimation of coefficients

The intermediate signal $z[n]$ for the two models is[2]:

$$z_W[n] = \sum_{m=0}^{M-1} h[m]x[n-m] \tag{3.14}$$

$$z_H[n] = \sum_{k=1}^{K} c_k x[n]|x[n]|^{k-1} \tag{3.15}$$

The baseband output of the two models is:

$$y_W[n] = \sum_{k=1}^{K} c_k \left[\sum_{m=0}^{M-1} h[m]x[n-m]\right] \left|\left[\sum_{m=0}^{M-1} h[m]x[n-m]\right]\right|^{k-1} \tag{3.16}$$

[2]Subscript denotes model: W for Wiener, H for Hammerstein

$$y_H[n] = \sum_{m=0}^{M-1} h[m] \left[\sum_{k=1}^{K} c_k x[n-m] |x[n-m]|^{k-1} \right] \tag{3.17}$$

In order to estimate the model coefficients with a linear estimation method, like the least-squares method, two sets of data vectors $(\mathbf{x}, \mathbf{y})$ are needed. These are denoted $(\mathbf{x}^{[1]}, \mathbf{y}^{[1]})$ and $(\mathbf{x}^{[2]}, \mathbf{y}^{[2]})$ respectively. The first set is used to find the coefficients for the first block. For the Wiener model the first set of coefficients are estimated using least-squares by:

$$\hat{\mathbf{a}} = (\mathbf{H}^H \mathbf{H})^{-1} \mathbf{H}^H \mathbf{y}^{[1]} \tag{3.18}$$

Where $\mathbf{a} = [h_0, \cdots, h_{M-1}]^T \in \mathbb{C}^M$ are the filter coefficients for a stable FIR-filter of order M and $\mathbf{H} \in \mathbb{C}^{N \times M}$ is the regression matrix for the first block, given by:

$$\mathbf{H} = \begin{bmatrix} x^{[1]}_{0,0} & x^{[1]}_{0,1} & \cdots & x^{[1]}_{0,M-1} \\ x^{[1]}_{1,0} & x^{[1]}_{1,1} & \cdots & x^{[1]}_{1,M-1} \\ \vdots & \vdots & \ddots & \vdots \\ x^{[1]}_{N-1,0} & x^{[1]}_{N-1,1} & \cdots & x^{[1]}_{N-1,M-1} \end{bmatrix} \tag{3.19}$$

Where $x_{n,m} = x[n-m]$.

Further, the second set of input data $\mathbf{x}^{[2]}$ is used to find the estimated intermediate signal $\hat{\mathbf{z}}$:

$$\hat{\mathbf{z}} = \mathbf{H}\hat{\mathbf{a}} \tag{3.20}$$

Where $\mathbf{H}$ is given in equation 3.19, but now constructed using $\mathbf{x}^{[2]}$ instead of $\mathbf{x}^{[1]}$.

The second set of coefficients is estimated by:

$$\hat{\mathbf{b}} = (\mathbf{G}^H \mathbf{G})^{-1} \mathbf{G}^H \mathbf{y}^{[2]} \tag{3.21}$$

Where $\mathbf{b} = [c_1, c_2, \cdots, c_K] \in \mathbb{C}^K$ are the coefficients of the non-linear complex polynomial of maximum order K, and $\mathbf{G} \in \mathbb{C}^{N \times K}$ is the regression matrix for the second block, given by:

$$\mathbf{G} = \begin{bmatrix} \hat{z}_{0,0} & \hat{z}_{0,1} & \cdots & \hat{z}_{0,K-1} \\ \hat{z}_{1,0} & \hat{z}_{1,1} & \cdots & \hat{z}_{1,K-1} \\ \vdots & \vdots & \ddots & \vdots \\ \hat{z}_{N-1,0} & \hat{z}_{N-1,1} & \cdots & \hat{z}_{N-1,K-1} \end{bmatrix} \tag{3.22}$$

Where $\hat{z}_{n,l} = \hat{z}[n]|\hat{z}[n]|^l$.

The Wiener model output is now found to be $\hat{\mathbf{y}} = \mathbf{G}\hat{\mathbf{b}}$. The total number of coefficients that needs computation is $\kappa_W = K + M$.

The same derivation can be performed for the Hammerstein model, only with the order of the two blocks switched. This is shown in [17], but is not shown here, as the scope of this thesis is not to give a full review of the derivation of these models.

3.2.4 Memory Polynomial Model

The memory polynomial model is described in [20] as a compromise between the memoryless non-linearity, and the full Volterra non-linearity. The model is derived by generalizing the Hammerstein model which involves choosing different filters for each non-linear order $k \in [1, \cdots, K]$ [21], thus incorporating non-linear memory in the Hammerstein model. This yields:

$$y_{GH}[n] = \sum_{k=1}^{K} \sum_{m=0}^{M-1} c_{k,m} x^{k-1}[n-m] \tag{3.23}$$

By selecting only combinations on the form $x[n]|x[n-m]|^{k-1}$, the baseband memory polynomial model from [22] is obtained:

$$y_{MP}[n] = \sum_{k=1}^{K} \sum_{m=0}^{M-1} c_{k,m} x[n-m]|x[n-m]|^{k-1} \tag{3.24}$$

This model has proven effective for predistortion of power amplifiers in [20, 21]. Additionally, it can be generalized to have potential for even better performance, which is done in [21] but not implemented in this thesis.

Estimation of coefficients

Expressed in matrix form, equation 3.24 becomes:

$$\mathbf{y} = \underline{\mathbf{H}}\mathbf{c} \tag{3.25}$$

where $\mathbf{c} \in \mathbb{C}^{\kappa_{MP}}$ are the coefficients and $\kappa_{MP} = K \times M$ is the total number of coefficients. $\underline{\mathbf{H}}$ is the memory polynomial model regression matrix given by:

$$\underline{\mathbf{H}} = \begin{bmatrix} \mathbf{X_0} \cdots \mathbf{X_{M-1}} \end{bmatrix} \in \mathbb{C}^{M \times \kappa_{MP}} \tag{3.26}$$

$\mathbf{X_m} \in \mathbb{C}^{N \times K}$ are given by:

$$\mathbf{X_m} = [\mathbf{x_{n,m,k}}, \mathbf{x_{n-1,m,k}}, \cdots, \mathbf{x_{n-(N-1),m,k}}]^T \tag{3.27}$$

where

$$\mathbf{x_{n,m,k}} = \left[x(n-m)|x(n-m)|^0, \cdots, x(n-m)|x(n-m)|^{K-1}\right]^T \tag{3.28}$$

Through least-squares estimation, the coefficients $\mathbf{c}$ can be estimated:

$$\hat{\mathbf{c}} = (\underline{\mathbf{H}}^H \underline{\mathbf{H}})^{-1} \underline{\mathbf{H}}^H \mathbf{y} \tag{3.29}$$

where $\mathbf{y} = [y_0, y_1, \cdots, y_{N-1}]^T$ is the output vector of N samples.

The model output $\hat{\mathbf{y}}$ is now:

$$\hat{\mathbf{y}} = \underline{\mathbf{H}}\hat{\mathbf{c}} \tag{3.30}$$

3.3 Validation of Models

Validating the different behavioral models is done by evaluating the normalized mean-square-error (NMSE) between the PA output $\mathbf{y}$ and the model output $\hat{\mathbf{y}}$. NMSE is defined as:

$$NMSE(\mathbf{y}, \hat{\mathbf{y}}) = 10log_{10}\left[\frac{\|\mathbf{y} - \hat{\mathbf{y}}\|_2^2}{\|\mathbf{y}\|_2^2}\right] \tag{3.31}$$

A lower NMSE means the model can better describe the PAs non-linear behavior and is expected to perform better at predistortion linearization.

Chapter 4

Digital Predistortion

This chapter explains the concept of digital predistortion and how to use it to linearize a power amplifier. Non-linear behavior in power amplifiers is one of the major challenges of modern communication systems. As complex digital modulation techniques have developed, linearity has become more and more critical to avoid distortion and information loss. Due to the importance of PA linearity, researchers have developed several methods to linearize their operation. Methods such as feed-forward, feed-back, and analog predistortion are earlier techniques which have only achieved modest results. In addition they are not very configurable and are often difficult to implement.

Modern high-speed digital circuitry has allowed the implementation of digital predistortion (DPD) techniques which have shown far greater linearity results than the earlier analog techniques. DPD techniques have the advantage of being highly configurable and cheap to implement, which have made them the most popular techniques for linearization in the later years.

The basic idea of digital predistortion is to cancel the non-linear distortion introduced by the power amplifier and achieve a linear relationship between input and PA output. This is achieved by performing a digital operation on the input signal which has the inverse characteristic of that of the PA, to ideally cancel all distortion introduced by the PA and thus achieve a linear response.

The critical challenge of DPD is obviously finding an accurate inverse of the PA behavior. This challenge is not a trivial one, as PAs usually have complex non-linearities and dynamic behavior due to memory effects. The linearity results of the DPD system thus depends on the chosen PA model. In this thesis, the behavioral models explained in chapter 3 are used as a basis for the DPD system.

4.1 The Linearization Problem

Figure 4.1 shows a block diagram of the digital predistortion system operation. The lower branch consists of the predistorter, N, and the non-linear RFPA, P. When excited with input signal $\mathbf{x} \in \mathbb{C}^N$, the lower branch produces the output signal $\mathbf{y}$. The upper branch consists of a linear operator, L, which applies a desired linear voltage gain G to the input signal $\mathbf{x}$, producing a signal $\mathbf{z} = G\mathbf{x}$. An ideal predistorter will cancel all non-linearities of the PA, resulting in $\mathbf{y} = \mathbf{z}$.

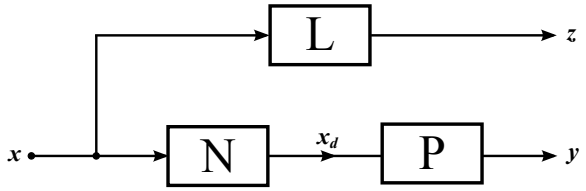

Figure 4.1: Illustration of the linearization problem for the DPD system.

The linearization problem of the predistortion operation is essentially to minimize the error between the system output $\mathbf{y}$, and the ideal linear output $\mathbf{z}$.

Assuming the PA can be described by one of the behavioral models explained in chapter 3, the system output $\mathbf{y}$ can be written as:

$$\mathbf{y} = \mathbf{Hc} \in \mathbb{C}^N \tag{4.1}$$

Where $\mathbf{H}$ is the model specific regression matrix constructed from the input signal $\mathbf{x}$, and $\mathbf{c}$ is the coefficient vector for the specific behavioral model.

In order to solve such a linearization problem it's important to understand that due to the PA's inherently non-linear behaviour, equation 4.1 is not in general possible to solve analytically. However, for a specific set of input signals around an operating point $\mathbf{x_0}$, there will usually be local solutions allowing linearization of the PA. These local solutions result in a pre-filter which are only an approximation to the inverse response of the PA for a limited set of input signals:

$$\big\|P\big[N[\mathbf{x}]\big] - L\big[\mathbf{x}\big]\big\|_2 < \epsilon, \quad \|\mathbf{x} - \mathbf{x_0}\| < \delta \tag{4.2}$$

Where ϵ and δ are small positive constants. In order to find the coefficients minimizing the error ϵ, it's important to note that they have a dependency on the predistorter structure N. This structure is not in general known, however assuming the PA may be modeled with sufficient accuracy using behavioral modeling, then the inverse characteristic may also be sufficiently modeled, meaning the coefficients may be estimated using least-squares estimation.

In this thesis, the indirect learning architecture (ILA) is used to estimate the predistorter characteristic, however several other techniques exist. The ILA method is chosen due to simplicity and acceptable documented results [12, 16].

4.2 The Indirect Learning Architecture

The indirect learning architecture is illustrated in figure 4.2. The feed-back path contains a post-inverse filter which can be used to estimate the coefficients for the DPD unit, which works as a pre-inverse filter. Martin Schetzen shows in [23] that the *p*th-order pre-inverse of a system $\mathbf{H}$ is identical to its *p*th-order post-inverse. Thus, by finding the coefficients of the post-inverse filter with $\mathbf{y}/G$ as its input and $\hat{\mathbf{x}}_\mathbf{d}$ as its output, the predistorted input can be found.

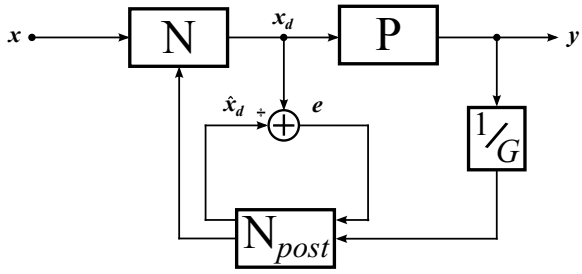

Figure 4.2: Block diagram illustrating the indirect learning architecture.

Assuming the operators N and N_{post} are equal as shown in [23], the error signal $\mathbf{e}$ can be expressed as:

$$\mathbf{e} = N\big[\mathbf{y}/G\big] - N\big[\mathbf{x}\big] = \mathbf{x_d} - \hat{\mathbf{x}}_\mathbf{d} \tag{4.3}$$

Achieving zero-error between the actual and estimated predistorted signals, i.e. $\mathbf{x_d} - \hat{\mathbf{x}}_\mathbf{d} = \mathbf{0}$, yields:

$$\frac{\mathbf{y}}{G} = \mathbf{x} \tag{4.4}$$

Which leads to the desired linear input/output relation:

$$\mathbf{y} = G\mathbf{x} \tag{4.5}$$

It's desirable to minimize the error $\mathbf{e}$ to achieve the closest match between the actual system output and the desired linear response in equation 4.5. The output $\hat{\mathbf{x}}_\mathbf{d}$ of the post-inverse filter N_{post} can be written as:

$$\hat{\mathbf{x}}_\mathbf{d} = \mathbf{H}_\mathbf{y}\mathbf{c}_\mathbf{post} \tag{4.6}$$

Where $\mathbf{H}_\mathbf{y}$ is the model specific regression matrix composed from the scaled output $\mathbf{y}/G$.

Finding the coefficients $\mathbf{c}_\mathbf{post}$ which minimize $\|\mathbf{e}\|_2^2$ using least-squares minimization explained in section 2.3 yields:

$$\hat{\mathbf{c}}_\mathbf{post} = (\mathbf{H}_\mathbf{y}{}^H\mathbf{H}_\mathbf{y})^{-1}\mathbf{H}_\mathbf{y}{}^H\mathbf{x}_\mathbf{d} \tag{4.7}$$

The predistorted signal $\mathbf{x}_\mathbf{d}$ can now be found as:

$$\mathbf{x}_\mathbf{d} = \mathbf{H}_\mathbf{x}\hat{\mathbf{c}}_\mathbf{post} \tag{4.8}$$

Where $\mathbf{H}_\mathbf{x}$ is the model specific regression matrix composed from the system input signal $\mathbf{x}$.

Thus, based on measurement data, the relation between output vector $\mathbf{y}$ and corresponding input $\mathbf{x}$ can be used to generate static predistortion coefficients.

4.3 Figures of Merit

The performance of the DPD operation will be evaluated mainly based on its ability to reduce out-of-band spectral regrowth and in-band distortion. Figures which describe these effects are the adjacent-channel-power ratio and the error-vector magnitude.

4.3.1 Adjacent-Channel-Power Ratio

Spectral regrowth is caused by intermodulation from non-linearities and can be reduced by predistortion. A figure of merit used to measure this reduction is hte adjacent-channel-power ratio (ACPR). ACPR is in this thesis computed as the ratio of the total power of the intermodulation distortion (IMD) bands and the total power of the main channel:

$$\text{ACPR}_i = 20log_{10}\left[\frac{\int\limits_{adjacent}|Y(f)|}{\int\limits_{main}|Y(f)|}\right] \tag{4.9}$$

Where *adjacent* denotes the adjacent channel, *main* denotes the main channel, and $Y(f)$ is the output power spectrum from the PA. The main channel is 10 MHz wide centered at $f = 0$ Hz. The adjacent channel spacing is set to 14.4 MHz and has a bandwidth of 10 MHz. The upper and lower third order intermodulation adjacent channels are shown in figure 4.3.

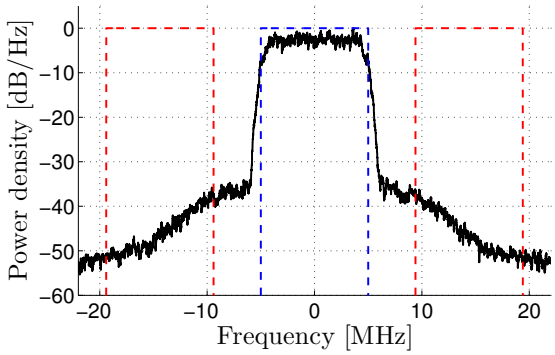

Figure 4.3: Main (blue) and adjacent (red) channels.

4.3.2 Error-Vector Magnitude

In-band distortion will be evaluated using error-vector magnitude (EVM). EVM is a way of describing the in-band distortion by looking at the magnitude of the error-vector between the optimal and received signal vectors at the correct sampling points. This is illustrated in figure 4.4.

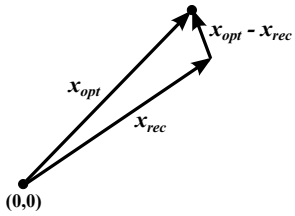

Figure 4.4: Illustration of error-vector magnitude.

The EVM definition used in this thesis is:

$$\text{EVM}_{\%} = \frac{mean\big(|\mathbf{x_{opt}} - \mathbf{x_{rec}}|\big)}{mean\big(|\mathbf{x_{opt}}|\big)} * 100\% \tag{4.10}$$

Where $\mathbf{x_{opt}}$ and $\mathbf{x_{rec}}$ are the optimal and received signal vectors respectively at the correct sampling points.

Chapter 5

Methodology

This chapter describes the approach when testing algorithms in MATLAB and performing measurements for PA characterization and predistortion. In order to thoroughly test the different models, behavioral modeling and predistortion linearization are performed on two different PAs with different operating frequencies.

The first is the Cree CMPA5585025F off-the-shelf GaN PA intended as the transmitter PA for the radar system, with a frequency band of 5.5 to 8.5 GHz. The second is a class F PA designed at NTNU, based on Cree's CGH40010F 10W GaN transistor with a frequency band of 1.8 to 2.6 GHz. It's biased in class AB, but harmonic tuning of the output matching network makes it class F. The two PAs are from here on referred to as *the 25W PA*, meaning the CMPA5585025F intended for the radar system, and *the 10W PA*, meaning the CGH40010F-based PA.

5.1 MATLAB

The predistortion algorithms are implemented and tested in MATLAB[1]. The 25W PA is an off-the-shelf product for which there exists no physical model describing its behavior. In order to test the algorithms in MATLAB, a single tone characterization of the 25W PA is performed. The AM/AM and AM/PM distortio data is imported to MATLAB and used to create a function emulating a signal being sent through the PA. This function returns the output signal $y[n]$ which together with input signal $x[n]$ is used to find the PA and predistortion coefficients as explained in chapters 3 and 4. This model is memoryless however, meaning the models' ability to model memory effects is not tested.

[1] Selected MATLAB code is found in appendix B

5.2 Characterization of the Power Amplifier

In order to perform digital predistortion on the PA, its non-linear behavior needs to be characterized and described with one of the behavioral models described in chapter 3. This characterization can be done in more than one way, e.g. by using a single-tone input signal, swiping the input power. This will reveal the static AM/AM and AM/PM distortion introduced by the PA. In order to excite the memory effects causing dynamic deviation in this distortion, a different signal is needed. By applying a signal with non-constant envelope, like a 16-QAM signal, these effects may be characterized.

5.2.1 Driver PAs

To drive the PAs as much as possible into compression, driver PAs are necessary. For the 25W PA, two drivers are used. This is because the first driver, a Hewlett Packard 83017A with a gain of ~ 35 dB, is not able to deliver enough output power to drive the PA very far into compression, before introducing too much distortion. It's desirable for the driver to operate as linearly as possible, while driving the DUT PA into compression such that the distortion at the output is clearly dominated by the DUT PA's non-linearities. This is unfortunately only the case for a limited set of input power levels, before the driver's distortion starts dominating. Therefore, a second driver is needed to deliver more output power. This second driver is a class A PA based on the same Cree's 10W GaN transistor and has a gain of ~ 6.5 dB at 8.25 GHz. A class A PA is biased in such a way that the transistor has a $360°$ conduction angle, and thus introduces minimal non-linear distortion, especially when operated far into back-off. The driver PA used for the 10W PA is also class A and based on the Cree 10W GaN transistor, with a gain of ~ 12 dB at 2.0 GHz.

5.2.2 Lab Equipment

The lab equipment used for measurements is:

- Vector Network Analyzer, Agilent E8364B
- Vector Signal Generator, Rohde & Schwarz SMU200A
- RF Source, Rohde & Schwarz SGS100A
- Signal Analyzer, Rohde & Schwarz FSQ40

5.2.3 PA Characterization Setup

Single tone measurements are performed as shown in figure 5.1. Using a power sweep on the VNA, the magnitude of the transmission parameter S_{21} as a function of input power is extracted. The frequency of the tone is 8.25 GHz for the 25W PA and 2.0 GHz for the 10W PA.

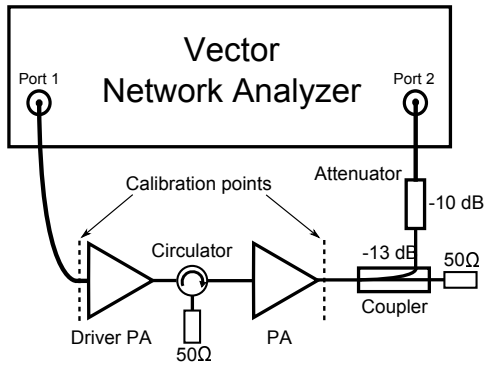

Figure 5.1: Setup for single tone measurements.

In order to characterize the PAs' dynamic AM/AM and AM/PM distortion, a 16-QAM signal is used as the input. The signal consists of random symbols generated in MATLAB, and is sent to the SMU200A vector signal generator via a LAN connection. The specifications of the 16-QAM input signal are shown in table 5.1.

Parameter	Value
Symbol rate	10 MHz
PAPR	6.4 dB
No. of symbols	2048
fs	100 MHz
Oversampling rate	5
Filter	Raised cosine
Filter roll-off	0.22
No. of samples	20880

Table 5.1: 16-QAM signal specifications

The 16-QAM signal is filtered with a raised cosine filter to avoid intersymbol interference. The measurement setup differs slightly for the two PAs. This is because the SMU200A is not able to up-convert the signal as high as 8.25 GHz which is the center frequency intended for the radar pulse. For the 25W PA, the SGS100A RF source receives the baseband 16-QAM signal from the SMU200A through separate channels for I and Q, and up-converts the signal to center frequency 8.25 GHz and delivers it to the PA. For the 10W PA, the center frequency is 2.0 GHz, and the up-converting operation can be performed by the SMU200A alone. The output signal $y[n]$ from the PAs is extracted by the FSQ40 signal analyzer and sent back to MATLAB, normalized to a maximum envelope of 1. The two signals $x[n]$ and $y[n]$ are aligned through cross-correlation, finding the best match between the two vectors. The gain G is then computed as the mean gain of normalized input envelope values below, 0.4, i.e. $\mathbf{x}/max|\mathbf{x}| < 0.4$. In order to keep the internal clocks of the generators and spectrum analyzer synced, the SMU200A's clock is used as a reference in order to avoid phase drift.

Measurement setups for the two PAs are as shown in figure 5.2. The 25W PA is biased with $V_{DS} = 28$ V and $I_{DS} = 285$ mA, and the 10W PA is biased with $V_{DS} = 28$ V and $I_{DS} = 160$ mA. Since the input impedance of the PAs can change as the input power

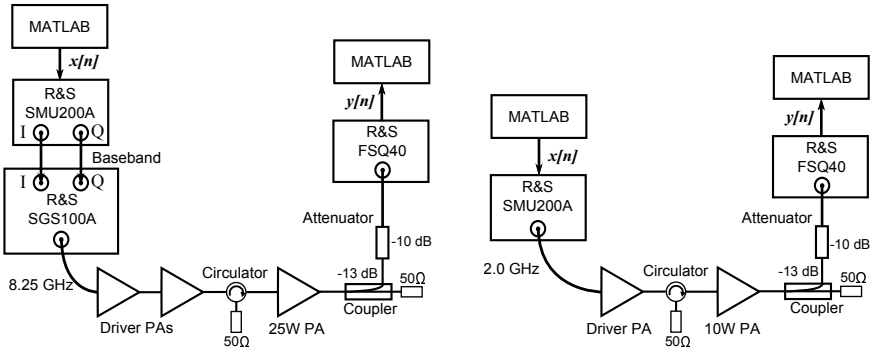

(a) Setup for 25W PA. **(b)** Setup for 10W PA.

Figure 5.2: Measurement setup for PA characterization using 16-QAM signal.

increases, a circulator is placed between the driver and the PA to ensure that the driver output sees no reflection. This means the driver output is always matched to 50Ω as the input power increases. The coupler and attenuator at the PA output are there to protect the VNA from the PAs' high power output levels. The coupler and circulator are terminated with 50Ω to ensure minimal reflection. The loss from the PA output to the signal analyzer was measured to be 25.0 dB at both 2.0 and 8.25 GHz. Both PAs are driven to the point where the driver's non-linearities become too severe to neglect.

Characterization is performed at different power levels, and after the PAs have been characterized, the predistortion coefficients are computed in MATLAB for each power level and applied to the input signal. The predistorted signal will now have an increased PAPR compared to the original signal, because the peaks which suffer from large amounts of compression have been increased to compensate. Driving the PA this hard will induce major non-linearities and memory effects not characterized. In order to avoid this, the increase in PAPR is limited to 3 dB above the original signal PAPR, and peaks above this are hard clipped. The predistorted signal is then sent to the signal generator. In addition to the 16-QAM signal from table 5.1, an OFDM signal consisting of 16 sub-carriers, is applied. The OFDM signal specifications are shown in table 5.2.

Parameter	Value
No. of sub-carriers	16
Sub-channel spacing	625 kHz
Bandwidth	10 MHz
PAPR	9 dB
Filter	Gaussian
Filter bandwidth-time product	0.8
No. of samples	20682

Table 5.2: ODFM signal specifications

The actual radar OFDM signal will have a bandwidth of 50 MHz, however the SMU200A signal generator has a maximum sampling rate of 100 MHz [8], which limits the bandwidth of the transmitted signal. The Nyquist criterion limits the bandwidth of the transmitted signal to 50 MHz, but as explained in section 2.7.1, a predistorted signal will have a larger spectral bandwidth than the original signal, meaning it will not be possible to predistort a signal with 50 MHz bandwidth with the lab equipment available in this thesis. Therefore the OFDM bandwidth has been reduced to 10 MHz to allow implementation of digital predistortion.

Chapter 6

Results

This chapter presents the behavioral modeling and linearization results. First, the different models' abilities to model the PA are validated by the achieved NMSE between the PA output $\mathbf{y}$ and the model output $\hat{\mathbf{y}}$. Then, the models are used to perform digital predistortion linearization and the results are presented. The linearization performance of the different models will be evaluated using ACPR and EVM as explained in section 4.3. Discussion and evaluation of the results follows in chapter 7.

The results are presented separately for PA modeling and linearization, and also for each of the two PAs. In each section, an introduction explains which kinds of measurements have been performed, and each PA subsection starts by explaining what can be seen in each figure. The different models are denoted CPS_K^{orders} for the complex power series, $MP_{K,M}^{orders}$ for the memory polynomial, $W_{K,M}^{orders}$ and for Wiener. K denotes the maximum non-linear order and M is the memory length, and $orders$ denotes which non-linear orders are included in the polynomial: odd-only or all.

The Hammerstein model implementation did not work as intended in practice in spite of numerous tests in MATLAB. It achieved somewhat reasonable modeling results, however it was unable to linearize through predistortion and instead resulted in more distortion than without predistortion. The results for the Hammerstein model has therefore not been included.

6.1 PA Modeling Results

Using the same 16-QAM signal for all measurements as specified in table 5.1 and the measurement setup shown in figure 5.2, the dynamic AM/AM and AM/PM characteristics of the two PAs are measured. The different models are then used to model the PA behavior

while varying non-linear orders keeping a constant memory length, and varying the memory length keeping a constant non-linear order. Each model's ability to describe the PA behavior is evaluated through the achieved $NMSE(\mathbf{y}, \hat{\mathbf{y}})$ as described in section 3.3. The models are evaluated up to a maximum non-linear order of $K = 9$ and memory length $M = 9$.

6.1.1 10W PA

Table 6.1 shows the measured specifications of the 10W PA. Figure 6.1 shows the power density spectra of the PA output at different values of average $\bar{P}_{out}$, and how spectral regrowth is affected by the output power. Figures 6.2 and 6.3 show $NMSE(\mathbf{y}, \hat{\mathbf{y}})$ for the different models using all or odd orders only. Figure 6.4 shows AM/AM and AM/PM distortion, modeled with the $MP^{all}_{4,3}$ model. The average power $\bar{P}_{out}$ is given for each figure and the RF center frequency for the measurements is 2.0 GHz.

Table 6.1: Measured specifications of the 10W PA at $f_c = 2.0$ GHz.

$\bar{\mathbf{P}}_{\mathbf{in}}$ [dBm]	$\bar{\mathbf{P}}_{\mathbf{out}}$ [dBm]	**Gain** [dB]	$\mathbf{ACPR}_{\mathbf{lower}}$	$\mathbf{ACPR}_{\mathbf{upper}}$ [dBc]
9.6	26.0	16.4	−49.7	−49.8
11.6	27.8	16.2	−45.9	−45.9
13.6	29.5	15.9	−43.0	−43.0
15.5	31.2	15.7	−41.4	−41.3
17.7	33.0	15.3	−40.9	−40.7
19.7	34.7	15.0	−40.6	−40.2
21.7	36.2	14.5	−39.4	−38.7
23.8	37.7	13.9	−36.1	−35.5

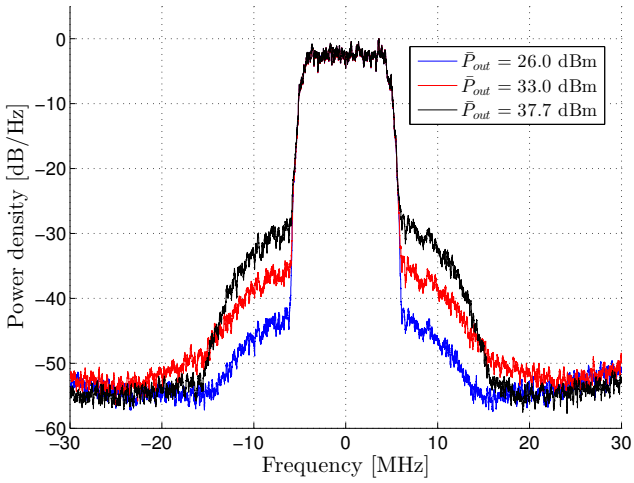

Figure 6.1: Normalized output power density spectra for 10W PA for different $\bar{P}_{out}$.

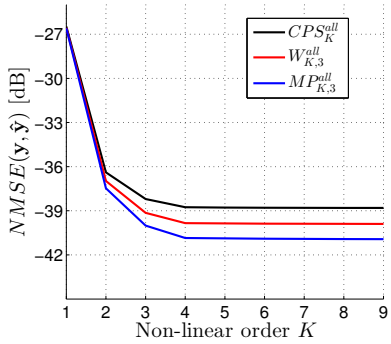

(a) Varying non-linear order, constant $M = 3$.

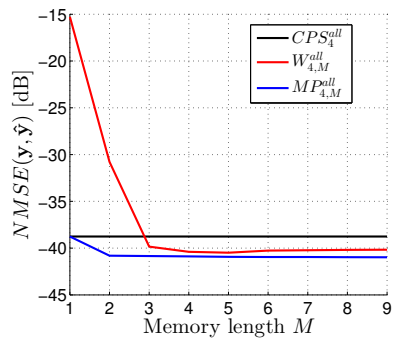

(b) Varying memory length, constant $K = 4$.

Figure 6.2: All orders, 10W PA, $NMSE(\mathbf{y},\hat{\mathbf{y}})$ for the different models, $\bar{P}_{out} = 36$ dBm.

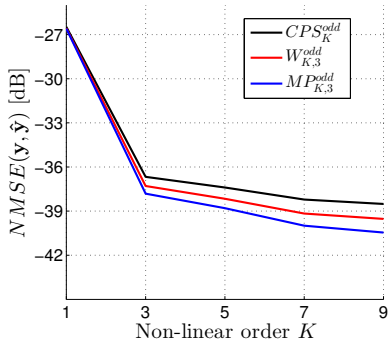

(a) Varying non-linear order, constant $M = 3$.

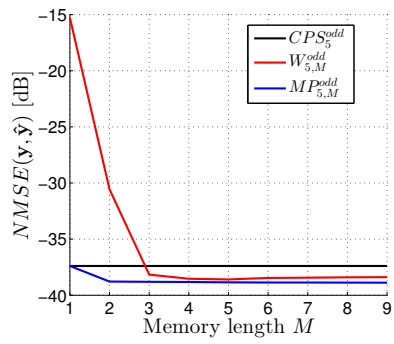

(b) Varying memory length, constant $K = 5$.

Figure 6.3: Odd orders only, 10W PA, $NMSE(\mathbf{y},\hat{\mathbf{y}})$ for the different models, $\bar{P}_{out} = 36$ dBm.

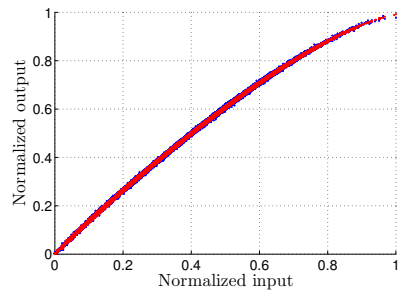

(a) AM/AM distortion.

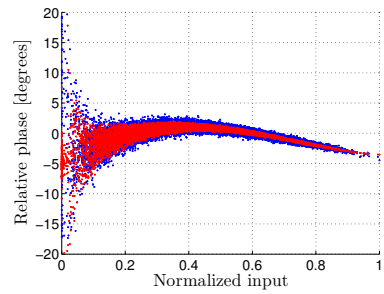

(b) AM/PM distortion.

Figure 6.4: Normalized non-linear distortion of 10W PA (blue) and $MP_{4,3}^{all}$ model output (red), $\bar{P}_{out} = 36$ dBm.

6.1.2 25W PA

Table 6.2 shows the measured specifications of the 25W PA. Figure 6.5 shows the power density spectra of the PA output at different values of average $\bar{P}_{out}$, and how spectral regrowth is affected by the output power. Figures 6.6 and 6.7 show $NMSE(\mathbf{y}, \hat{\mathbf{y}})$ for the different models using all or odd orders only. Figure 6.8 shows AM/AM and AM/PM distortion, modeled with the $MP_{4,3}^{all}$ model. The average power is given for each figure, and the RF center frequency is 8.25 GHz.

Table 6.2: Measured specifications of the 25W PA at $f_c = 8.25$ GHz.

$\bar{\mathbf{P}}_{\mathbf{in}}$ [dBm]	$\bar{\mathbf{P}}_{\mathbf{out}}$ [dBm]	**Gain** [dB]	$\mathbf{ACPR}_{\mathbf{lower}}$	$\mathbf{ACPR}_{\mathbf{upper}}$ [dBc]
5.1	25.1	20.0	−35.6	−38.3
7.1	26.4	19.3	−35.9	−37.3
9.0	27.7	18.7	−35.6	−36.4
11.0	28.8	17.8	−33.8	−37.0
12.8	30.0	17.2	−33.1	−37.3
14.7	31.5	16.8	−32.6	−37.7
16.6	33.7	17.1	−35.6	−38.2
18.5	34.9	16.4	−34.6	−36.0

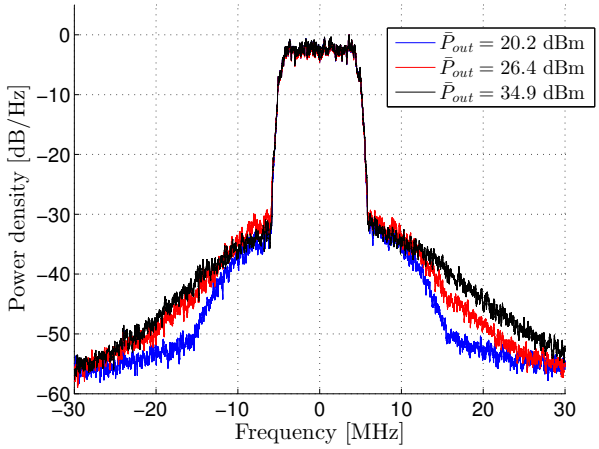

Figure 6.5: Normalized output power density spectra for 25W PA for different $\bar{P}_{out}$.

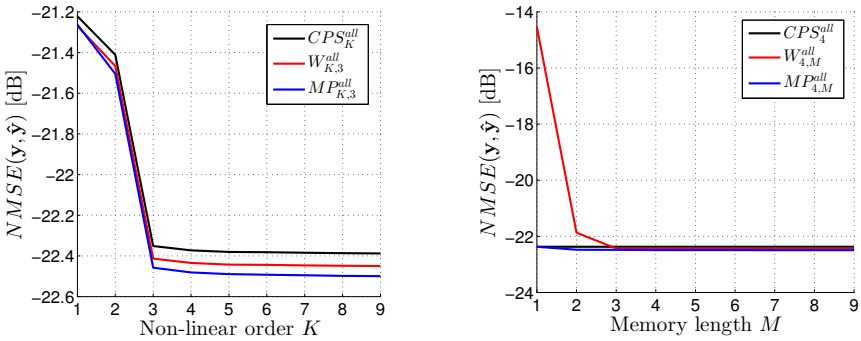

(a) Varying non-linear order, constant $M = 3$. **(b)** Varying memory length, constant $K = 4$.

Figure 6.6: All orders, 25W PA, $NMSE(\mathbf{y}, \hat{\mathbf{y}})$ for the different models, $\bar{P}_{out} = 33.7$ dBm.

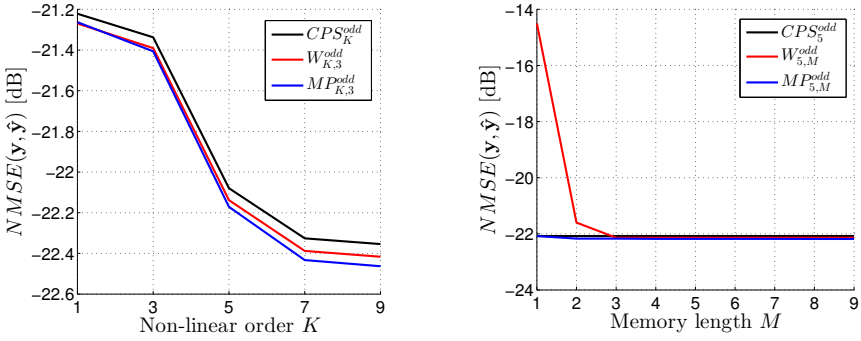

(a) Varying non-linear order, constant $M = 3$. **(b)** Varying memory length, constant $K = 5$.

Figure 6.7: Odd orders only, 25W PA, $NMSE(\mathbf{y}, \hat{\mathbf{y}})$ for the different models, $\bar{P}_{out} = 33.7$ dBm.

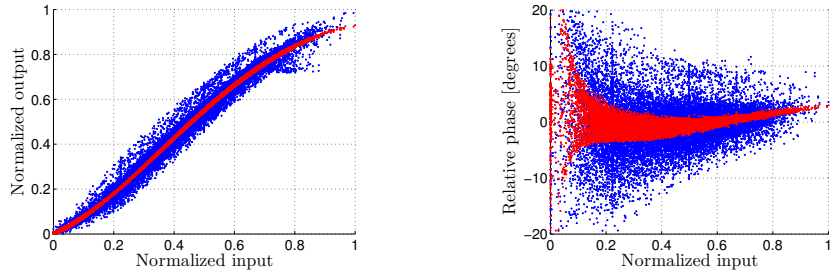

(a) AM/AM distortion. **(b)** AM/PM distortion.

Figure 6.8: Normalized non-linear distortion of 25W PA (blue) and $MP_{4,3}^{all}$ model output (red), $\bar{P}_{out} = 33.7$ dBm.

6.2 Linearization Results

Linearization is performed both using a 16-QAM signal and an OFDM signal. The specifications of these signals are found in tables 5.1 and 5.2. Since using all orders of the non-linear polynomial gave better modeling results, predistortion was only performed using all orders.

6.2.1 10W PA

16-QAM Signal

Figures 6.9 and 6.10 shows ACPR and EVM of the linearized output as functions of non-linear order K and memory length M respectively. Figures 6.11 and 6.12 show the ACPR and EVM of the original and linearized output signals as a function of average output power $\bar{P}_{out}$. Figure 6.13 shows the PA output power spectra before and after linearization. Figure 6.14 shows the 16-QAM constellation diagram before and after linearization. Figure 6.15 shows the AM/AM and AM/PM distortion of the linearized PA output compared to the original output.

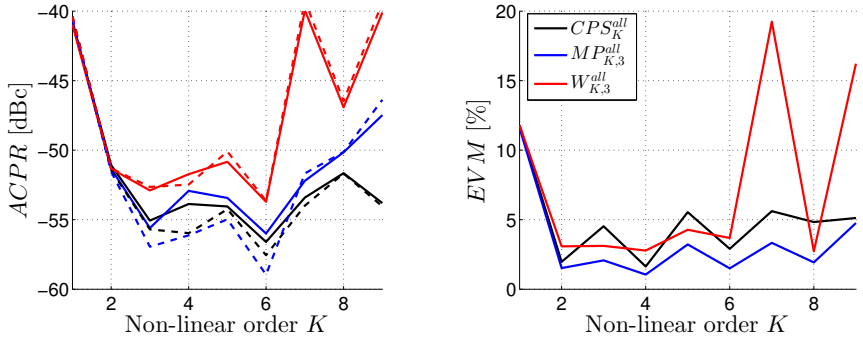

(a) $ACPR$, solid and dashed lines represent lower and upper channel respectively.

(b) $EVM_{\%}$

Figure 6.9: ACPR and EVM of linearized 10W PA output signals as functions of maximum non-linear order K, $\bar{P}_{out} = 33$ dBm.

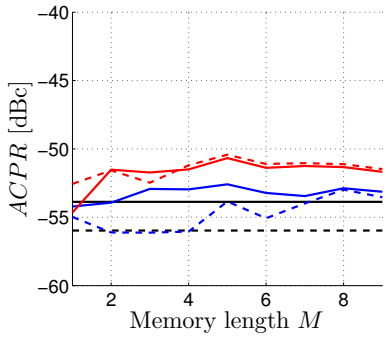

(a) $ACPR$, solid and dashed lines represent lower and upper channel respectively.

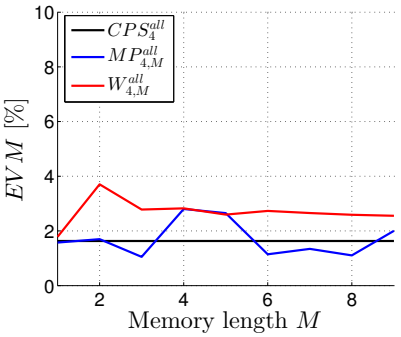

(b) $EVM_{\%}$

Figure 6.10: ACPR and EVM of linearized 10W PA output signals as functions of memory length M, $\bar{P}_{out} = 33$ dBm.

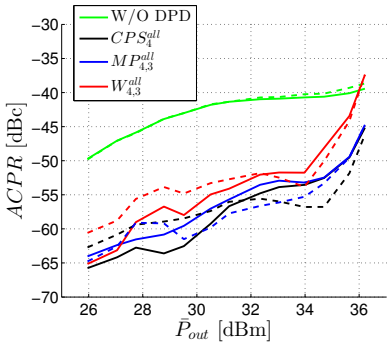

(a) Non-linear order $K = 4$.

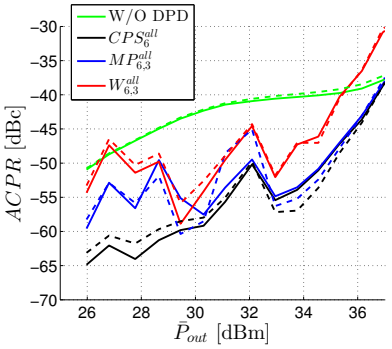

(b) Non-linear order $K = 6$.

Figure 6.11: ACPR of original and linearized 10W PA outputs, as functions of $\bar{P}_{out}$, solid lines represent lower channel, and dashed lines represent upper channel.

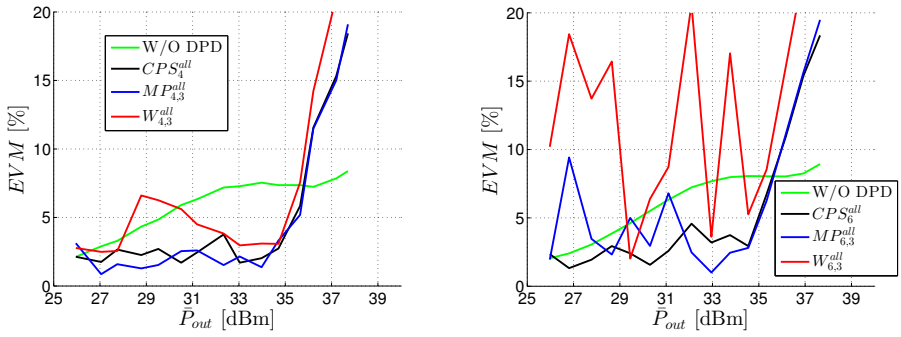

(a) Non-linear order $K = 4$.

(b) Non-linear order $K = 6$.

Figure 6.12: EVM as a function of $\bar{P}_{out}$ for linearized 10W PA output.

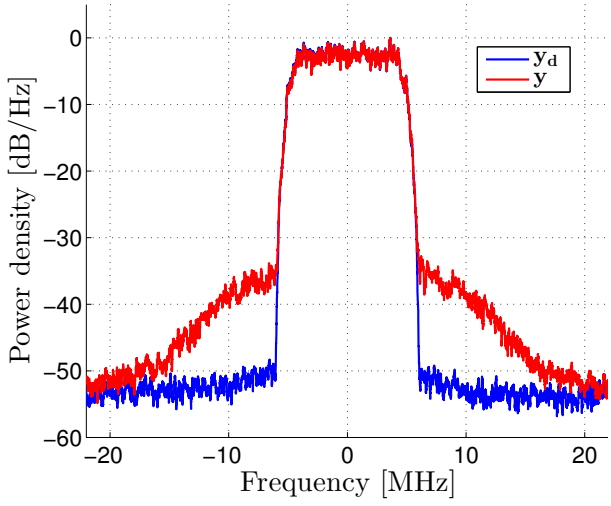

Figure 6.13: Normalized power density spectra for 10W PA with original $\mathbf{y}$ and linearized $\mathbf{y_d}$ output using $MP_{4,3}^{all}$ model, $\bar{P}_{out} = 33$ dBm.

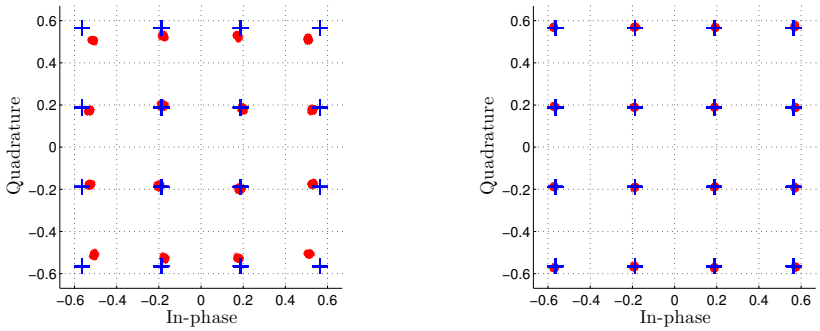

(a) Without predistortion. **(b)** With predistortion.

Figure 6.14: 16-QAM constellation diagram for 10W PA, optimal (blue) and measured (red) points, predistortion is done using the $MP_{4,3}^{all}$ model, $\bar{P}_{out} = 33$ dBm.

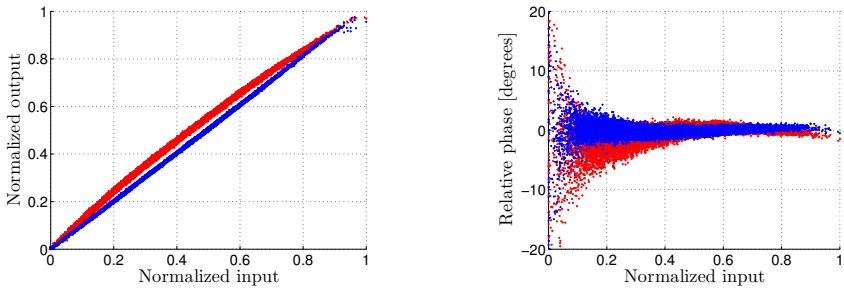

(a) AM/AM distortion. **(b)** AM/PM distortion.

Figure 6.15: Normalized non-linear distortion of 10W PA without predistortion (red) and with predistortion (red) using $MP_{4,3}^{all}$ model, $\bar{P}_{out} = 33$ dBm.

OFDM Signal

Figure 6.16 shows the ACPR of the original and the linearized output as functions of average output power $\bar{P}_{out}$. Figure 6.17 shows the output power spectra before and after linearization. Figure 6.18 shows the AM/AM and AM/PM distortion of the linearized PA output compared to the original output.

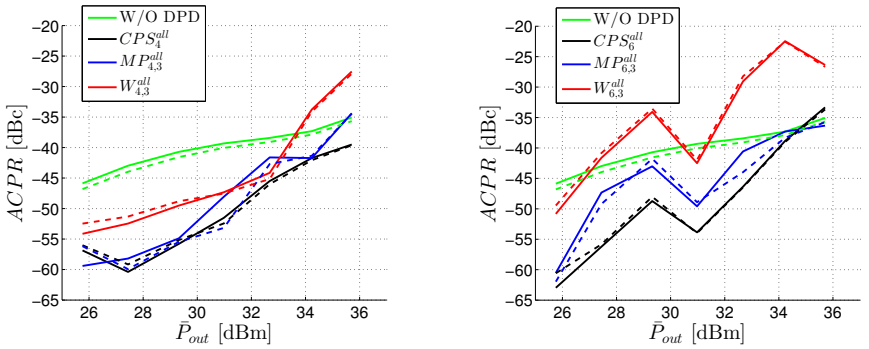

(a) Max non-linear order $K = 4$.

(b) Max non-linear order $K = 6$.

Figure 6.16: ACPR of original and linearized OFDM 10W PA outputs, as functions of $\bar{P}_{out}$, solid lines represent lower channel, and dashed lines represent upper channel.

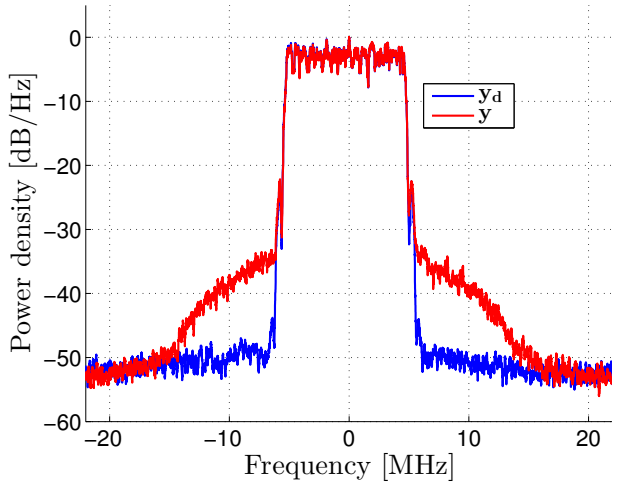

Figure 6.17: Normalized power density spectra of original $\mathbf{y}$ and linearized $\mathbf{y_d}$ OFDM 10W PA output using $MP_{4,3}^{all}$ model, $\bar{P}_{out} = 29.5$ dBm.

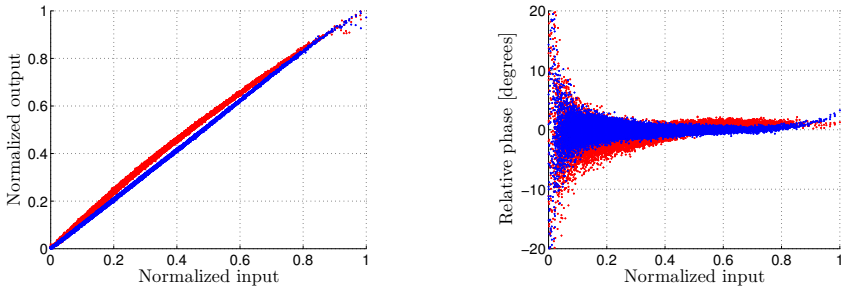

(a) AM/AM distortion.

(b) AM/PM distortion.

Figure 6.18: Normalized non-linear distortion of OFDM signal, 10W PA without predistortion (red) and with predistortion (red) using $MP_{4,3}^{all}$ model, $\bar{P}_{out} = 29.5$ dBm.

6.2.2 25W PA

16-QAM Signal

Figures 6.19 and 6.20 shows ACPR and EVM of the linearized output as functions of non-linear polynomial order K and memory length M respectively. Figure 6.21 shows the ACPR and EVM of the original and linearized output signals as a function of average output power $\bar{P}_{out}$. Figure 6.22 shows the PA output power spectra before and after linearization. Figure 6.23 shows the 16-QAM constellation diagram before and after linearization. Figure 6.24 shows the AM/AM and AM/PM distortion of the linearized PA output compared to the original output.

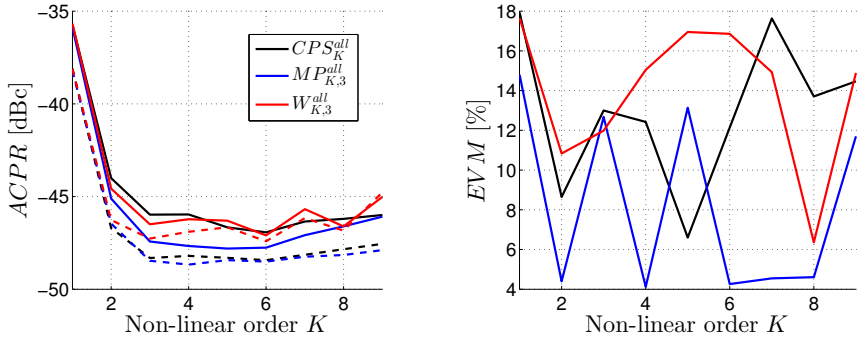

(a) $ACPR$, solid and dashed lines represent lower and upper channel respectively.

(b) $EVM_{\%}$

Figure 6.19: ACPR and EVM of linearized 25W PA output signals as functions of maximum non-linear order K, $\bar{P}_{out} = 23.5$ dBm.

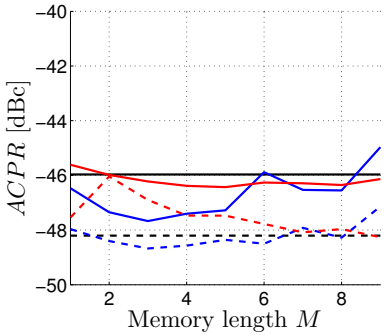

(a) $ACPR$, solid and dashed lines represent lower and upper channel respectively.

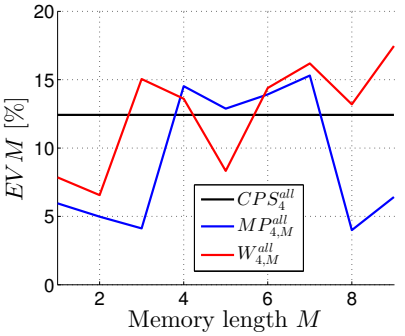

(b) $EVM_{\%}$

Figure 6.20: ACPR and EVM of linearized 25W PA output signals as functions of memory length M, $\bar{P}_{out} = 23.5$ dBm.

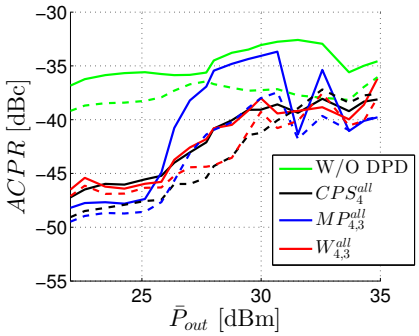

(a) $ACPR$, solid and dashed lines represent lower and upper channel respectively.

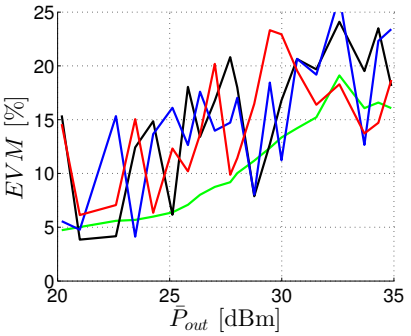

(b) $EVM_{\%}$

Figure 6.21: ACPR and EVM of linearized 25W PA output signals as functions of $\bar{P}_{out}$.

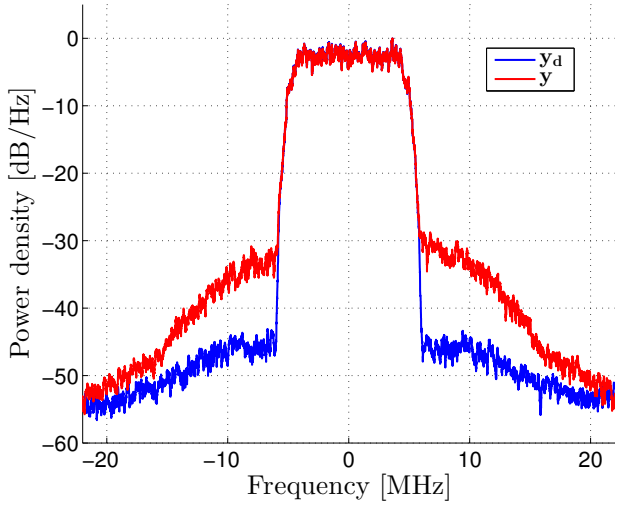

Figure 6.22: Normalized power density spectra of original $\mathbf{y}$ and linearized $\mathbf{y_d}$ 25W PA outputs, $\bar{P}_{out} = 23.5$ dBm.

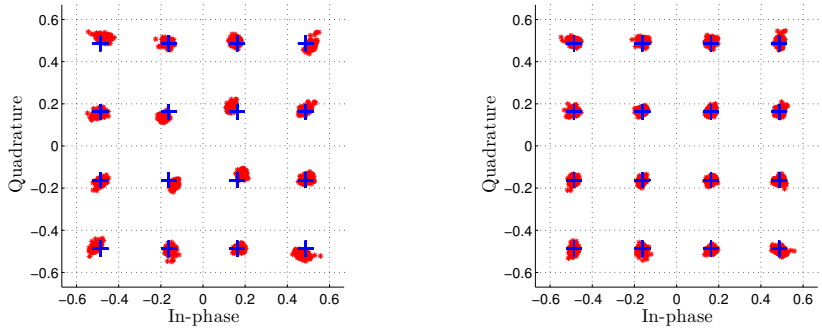

(a) Without predistortion. **(b)** With predistortion.

Figure 6.23: 16-QAM constellation diagram for 25W PA, optimal (blue) and measured (red) points, predistortion is done using the $MP^{all}_{4,3}$ model, $\bar{P}_{out} = 23.5$ dBm.

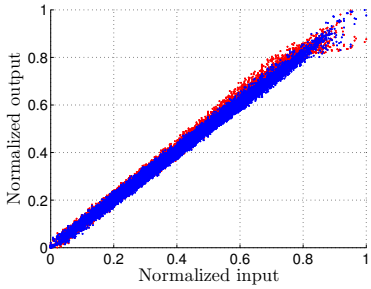

(a) AM/AM distortion.

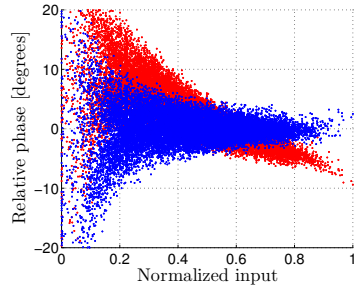

(b) AM/PM distortion.

Figure 6.24: Normalized non-linear distortion of 25W PA without predistortion (red) and with predistortion (red) using $MP_{4,3}^{all}$ model, $\bar{P}_{out} = 23.5$ dBm.

OFDM Signal

Figure 6.25 shows the ACPR of the original and the linearized output as functions of average output power $\bar{P}_{out}$. Figure 6.26 shows the output power spectra before and after linearization. Figure 6.27 shows the AM/AM and AM/PM distortion of the linearized PA output compared to the original output.

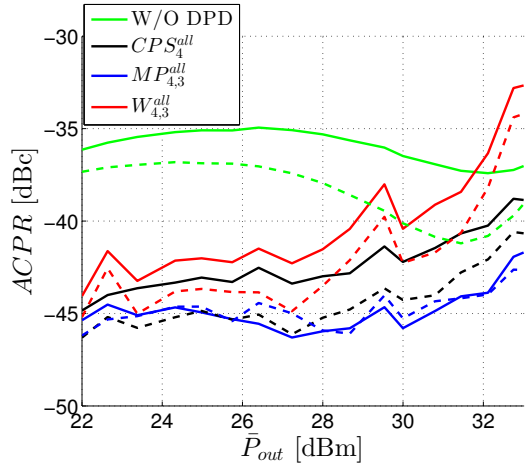

Figure 6.25: ACPR of original and linearized OFDM 25W PA outputs, as functions of $\bar{P}_{out}$, solid lines represent lower channel, and dashed lines represent upper channel.

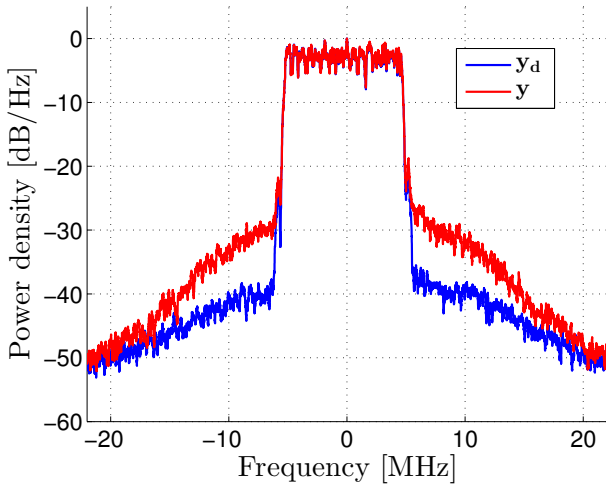

Figure 6.26: Normalized power density spectra of original $\mathbf{y}$ and linearized $\mathbf{y_d}$ OFDM 25W PA output using $MP_{4,3}^{all}$ model, $\bar{P}_{out} = 25.8$ dBm.

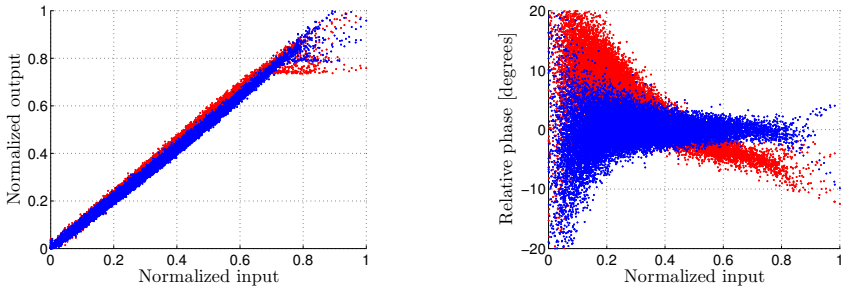

(a) AM/AM distortion.

(b) AM/PM distortion.

Figure 6.27: Normalized non-linear distortion of OFDM signal, 25W PA without predistortion (red) and with predistortion (red) using $MP_{4,3}^{all}$ model, $\bar{P}_{out} = 29.5$ dBm.

Chapter 7

Discussion

This chapter discusses the results from chapter 6. The most important topics for discussion are the different behavioral models' linearization performance relative to their computational complexity and also the increased spectral bandwidth as this is a major limiting factor when performing predistortion in the radar system. When discussing results, references will be made to figures in chapter 6, which will require some page flipping.

7.1 PA Modeling Through Behavioral Models

The PA modeling results are found in section 6.1. Figures 6.1 and 6.5 show that increasing the output power leads to an increase in spectral regrowth. The main difference between how this effect occurs in the two PAs, is that the 25W PA seems to be more non-linear than the 10W PA, and introduces more non-linear distortion. Even for low output powers, the 25W PA has quite high third order IMD, and increasing the power introduces quite high values of fifth order IMD as well, which is not seen for the 10W PA. The 25W PA also has more asymmetry in between the lower and upper adjacent channels. This can most likely be traced to large amounts of AM/PM distortion even at low power levels, shown e.g. in figure 6.8b, which as explained in section 2.4 will produce intermodulation products in the odd order harmonic bands.

Figures 6.2 and 6.6 reveal that the memory polynomial model achieves the best modeling performance at an $NMSE(\mathbf{y}, \hat{\mathbf{y}})$ of -41 dB for the 10W PA, and -22.5 dB for the 25W PA. Measurements on the 25W PA was found to give a much larger spread than the 10W PA, visible e.g. from figure 6.8a. This spread was present on all measurements for the 25W PA, but varied slightly from one measurements to the next, and although measurements were run up to 20 times for each power level, no better results than the ones presented were obtained. This suggests that the 25W PA suffers from much more severe memory effects than the 10W PA, making behavioral modeling harder. Even for models

incorporating memory effects, the $NMSE(\mathbf{y}, \hat{\mathbf{y}})$ does not improve drastically compared to the memoryless CPS model, even when increasing the memory length M of the models. This is elaborated further in section 7.2, but can most likely be traced to non-linear memory effects due to bias circuitry modulation causing AM/PM distortion which further causes asymmetry in sidebands. An additional reason for the larger spread might also be the additional noise introduced due to the use of two drivers as opposed to one for the 10W PA.

It's clear that little modeling improvement is achieved from using non-linear orders higher than $K = 4$, or a memory length of more than $M = 3$, as $NMSE(\mathbf{y}, \hat{\mathbf{y}})$ for all of the models flatten out for higher values of K and M. The memoryless CPS model has the worst performance, showing that it's beneficial to include memory in the models, suggesting that memory effects are present in the PAs.

From figures 6.3 and 6.7 it's clear that only using odd orders of the polynomial gives a less accurate model of the PAs as $NMSE(\mathbf{y}, \hat{\mathbf{y}})$ values are higher when using odd orders only as opposed to using all orders. This suggests that both PAs introduce orders of non-linear distortion which even order non-linearities are better at describing than odd orders, as an odd order polynomial requires a much higher degree to achieve the same $NMSE(\mathbf{y}, \hat{\mathbf{y}})$ results.

Based on the modeling results, a higher non-linear order than $K = 4$ is not expected to give any drastic linearization improvements. In the same manner, linearization is not expected to improve significantly when using a memory length of more than $M = 3$. When implementing predistortion to the radar system, it's desirable to achieve the best performance with as low maximum order K and memory length M as possible. This is both to reduce computational complexity, but also because signals predistorted with smaller values of K and M will have a smaller spectral bandwidth which will ease the constraints on both the digital and the analog electronics of the system. The importance of this issue is discussed further in section 7.4. Minimizing the number of coefficients which need computation is desirable, however this issue might not be a critical one. In the radar system predistortion is mainly implemented to investigate the benefits of linearization. Due to this experimental nature, the predistortion implementation will only use static coefficients that can be updated once in a while, allowing the computational complexity to be higher as coefficients are not computed that often. This would be a much more critical issue for a system using adaptive coefficient updating. The MP model is the most complex of the three with a total number of $\kappa_{MP} = K \times M$ coefficients. The W model has a total of $\kappa_W = K + M$ coefficients, and the CPS model has $\kappa_{CPS} = K$ coefficients. Thus, the models perform in scale of their complexity, which is a sensible result.

7.2 Digital Predistortion Linearization

7.2.1 ACPR and EVM

The linearization results are found in section 6.2. For the 10W PA, figures 6.9 and 6.10 show how the ACPR and EVM of the 16-QAM signal is affected by predistortion linearization with different values of maximum non-linear order K and memory length M, at one specific output power. Based on these figures it would seem that a non-linear order of $K = 6$ and memory length $M = 3$ would yield the best result, however figure 6.11 shows that a model with $K = 4$ and $M = 3$ yields a more stable linearization performance as the output power varies, and was found to give the best results overall. This instability is seen from the large variation in ACPR as power increases in figure 6.11b. The same can be said for the EVM shown in figure 6.12. This leads to a conclusion that the behavioral models are more sensitive as their complexity increases. It seems that performing predistortion also cause asymmetries in the lower and upper IMD sidebands which are not present without predistortion. This is seen in figure 6.11 where difference between the upper and lower IMD bands can be as much as 5 dB after predistortion although the uncorrected 10W PA has almost no asymmetry. This effect is present for all models, memoryless or otherwise. A single-tone characterization shown in appendix A shows that the 1-dB compression point of the 10W PA is at 33 dBm, at which point predistortion was able to reduce ACPR by 15 dB for the 16-QAM signal, but only about 5 dB for the OFDM signal, most likely due to the increased PAPR of the OFDM signal. EVM is reduced by 5% for the 16-QAM signal. The linearization gradually worsens as the output power increases, as predistortion is not able to correct the severe non-linearities occurring when the PA is far into compression.

For the 25W PA the best linearization performance was also found to be models with $K = 4$ and $M = 3$, however as mentioned in section 7.1, the characterization of the 25W PA behavior was much less accurate than for the 10W PA, with an $NMSE(\mathbf{y}, \hat{\mathbf{y}})$ of only -22.5 dB, naturally leading to lower linearization performance. Figure 6.21 shows ACPR and EVM reduction for the 16-QAM signal by more than 10 dB and 3% respectively using the $MP^{all}_{4,3}$ model for output power levels below 25 dB, however past this, the CPS^{all}_4 model achieves the best performance. The EVM reduction however is not very clear, as seen in figure 6.21b. There is a huge variation in EVM as the power output increases, and the main reason for this was the large spread in measurements on the 25W PA. This spread, visible e.g. in figure 6.8a, was present on all measurements for the 25W PA, but varied randomly from one measurement to the next. Extracting the best measurement from 20 runs per power level still did not yield any better results, meaning it's hard to confidently conclude that EVM has actually been reduced. EVM is calculated on the received PA output vector in MATLAB, leading to a suspicion that this is an issue occurring when the data is dumped from the signal generator and back to MATLAB. The ACPR results are computed by the FSQ40 signal analyzer directly and are more confident. It's clear that also for the 25W PA, predistortion can introduce IMD asymmetry, however the uncorrected 25W PA has quite large asymmetries by itself. The single-tone characterization in appendix A shows that the 1-dB compression point of the 25W PA is at 30 dBm, at which point pre-

distortion was able to reduce ACPR by no more than 6 dB for the lower and even less for the upper channel, with the 16-QAM input. The ACPR of the OFDM signal was reduced slightly more, by up to 10 dB for the lower, and 5 dB for the upper channel, which is a surprising result as the OFDM signal had a PAPR of 9 dB compared to 6.4 dB for the 16-QAM signal. This again only goes to show how sensitive the predistortion operation is with regard to the PA characterization results, which for the 25W PA proved less accurat than for the 10W PA. The linearization performance was better for lower output powers, with a maximum ACPR reduction of more than 10 dB for average output powers below 28 dBm.

The most important issue for getting good linearization results was found to be good characterization measurements of the PAs. Behavioral models are very sensitive to measurement noise and inaccuracies, and this was a major issue in the 25W PA. This suggests that the PA has large amounts of non-linearity and memory effects which even models with memory have a hard time describing, leading to lower linearization performance than for the 10W PA. An effect also suggesting large amounts of memory effects in the 25W PA is seen in the asymmetric lower and upper ACPR values in figures 6.21a and 6.25 showing a difference of up to 5 dB between channels. As explained in [2], and mentioned in section 2.4.3, this usually comes from modulation of bias circuitry. In [3, p.98] this is elaborated further, showing that sideband asymmetry can be traced to AM/PM distortion. This is very interesting, as it was clearly observable that the AM/PM distortion of the 25W PA was much more severe than for the 10W PA, and the 10W PA showed much more symmetrical IMD sidebands.

7.2.2 16-QAM Constellation Diagram

The reduction of EVM for the 10W PA is clearly visible in the constellation diagrams in figure 6.14, where the measured points are closer to the optimal points after linearization. The diagram is plotted at the 1-dB compression point where there are degrees of both AM/AM and AM/PM distortion, resulting in compression of the outer most measured points, and a phase shift of the measured points is visible as well. Digital predistortion is able to correct both the AM/AM and AM/PM distortion and reduce the EVM.

For the 25W PA, the constellation diagram shown in figure 6.23 is for a power level quite well below the 1-dB compression point. The reason for this was due to the large spread in measurements, and figures for higher power levels did not clearly illustrate how predistortion improved the constellation. However, for lower power levels, the distortion introduced by the 25W PA is dominated by large amounts of AM/PM distortion, which is clearly visible in the diagram without predistortion. After linearization the AM/PM distortion has been corrected and the points are closer to the optimal points.

7.2.3 AM/AM and AM/PM Distortion

The main characteristic separating the two PAs is that the 25W has quite severe AM/PM distortion even at low power outputs compared to the 10W PA. This is visible in figure

6.24b compared to 6.15b. The result of this is relatively high ACPR values, -35.6 dBc, even for the lowest power outputs, as seen in table 6.2 compared to -49.7 dB in table 6.1 for the 10W PA, and an asymmetry in lower and upper sidebands. Most of the ACPR and EVM reductions at low power levels come from linearizing the phase of the 25W PA output.

The linearization of the input/output characteristic of the 10W PA is clearly visible in figure 6.15 where the AM/AM distortion is much more linear and the relative phase shift between the input and output vectors is closer to zero. In figure 6.24 the linearization improvement of the 25W PA is not equally clear. The power level for which the AM/AM distortion has been plotted is not high enough that the PA has started to compress, yet the AM/PM distortion is quite severe. After linearization this is improved, in addition to a linear AM/AM response.

It was expected that the PA modeling and linearization results would match in such a way that the model performing the best in PA modeling would also be the best for predistortion. This was found to untrue, as the CPS model actually outperformed the two models in some cases, even though it had the worst performance in PA modeling. This shows that the added complexity introduced by the two models incorporating memory increases their sensitivity and might result in lower linearization performance.

7.3 Comments on Efficiency Enhancement

As mentioned before, the scope of this thesis does not include a detailed analysis of the efficiency enhancement benefits of performing digital predistortion linearization. However, some comments on the possibilities are appropriate.

7.3.1 10W PA

Figure 7.1 shows the single-tone power-added efficiency of the 10W PA and the ACPR values obtained on the OFDM signal with predistortion[1]. If an upper limit of an adjacent-channel power ratio is set to -45 dBc, $\bar{P}_{out}$ can be increased from 26 to 33 dBm using predistortion with the CPS_4^{all} model. Keeping in mind that the PAE data is from single-tone measurements it still indicates that the PAE can potentially be increased significantly by increasing the output power. However as an efficiency analysis was not performed on the 16-QAM or OFDM signals, no conclusion can be drawn as to the actual efficiency benefits of linearization.

[1]The PAE measurements were performed by Richard Samuelsen, designer of the 10W PA used in this thesis and are plotted with his courtesy.

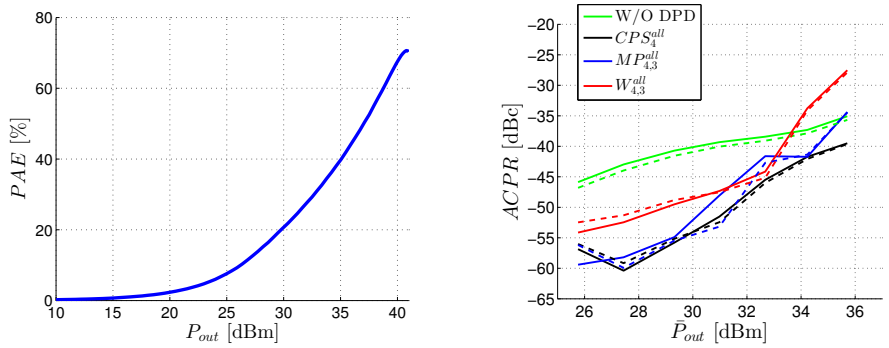

(a) Single-tone PAE of 10W PA at 2.0 GHz.

(b) $ACPR$

Figure 7.1: PAE of 10W PA and ACPR of OFDM outputs with predistortion.

7.3.2 25W PA

For the 25W PA it was shown in figure 6.25 that for the OFDM signal, both upper and lower ACPR values have been reduced to -45 dBc for a quite wide dynamic range for the 25W PA using the $MP_{4,3}^{all}$ model for predistortion. Figure 7.2 is collected from the 25W PA data sheet [24] and shows linearity and PAE of as functions of output power. Although

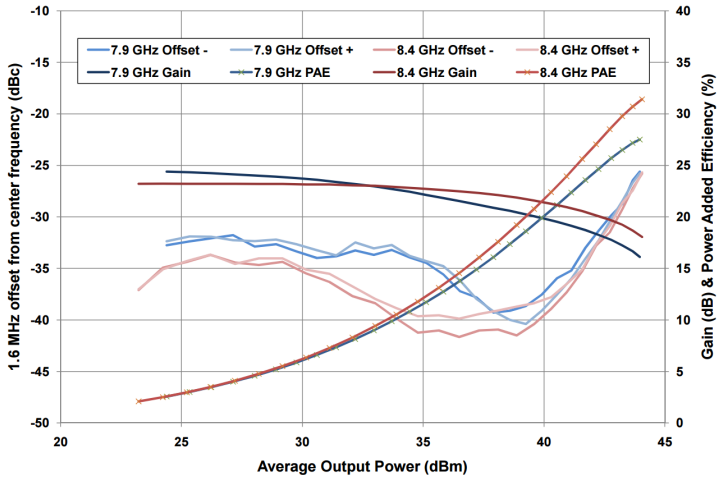

Figure 7.2: CMPA5585025F X-band Linearity, Gain, and PAE vs Average Output Power, $V_{DS} = 28$ V, $I_{DS} = 285$ mA, Offset-QPSK, 1.6 Msps [24, p.6].

the signal applied here is a OQPSK signal with much lower PAPR than the signals used in this thesis, and with a bandwidth of only 1.6 MHz, the linearity results are comparable to those obtained in this thesis, showing ACPR values between -35 and -42 dBc for output power levels from 25 to 34 dBm. By reducing these by 10 to 5 dB through DPD, the PA

can be driven slightly harder before reaching these values, which will slightly increase the PAE of the PA. This increase will however most likely be small. In figure 6.25 it's shown that for average output power levels of 30 dBm and above the ACPR for the predistorted output starts to increase and the ACPR reduction from predistortion relative to the original output will likely be consumed within a few dB of extra output power. Looking at the PAE curve in figure 7.2 shows that there are not much efficiency to gain from adding a couple of dB past the 30 dBm mark.

Exactly how much harder the PA can be driven is only speculation, however, as the PA was not driven harder than an average output power of 33 dBm for the OFDM signal due to the non-linearities introduced by the drivers past this. It can also be said that the efficiency enhancement will depend on the application and its upper limits of non-linearity. These comments were aimed at the radar system in question, where the desired output power is as high as possible.

7.4 Limitations of Digital Predistortion

Digital predistortion linearization has many benefits and has achieved better results than traditional linearization techniques such as feed-forward, feed-back, and analog predistortion. DPD is very versatile, however there are some limitations that are important to consider.

The first limitation is the increased computational complexity required to compute the coefficients from characterization of the PA. For adaptive algorithms updating coefficients during operation, this might introduce a constraint, however for the experimental radar system in question in this thesis the thought is to use static coefficients that can be computed once in a while, instead of adaptively updating them. This reduces the limitation that computational complexity puts on the system.

A second, and for the radar system very important, limitation of DPD is the increased bandwidth of the predistorted signal compared to the original signal. To cancel the PA's intermodulation distortion, the predistorter introduces intermodulation products, increasing the spectral bandwidth of the signal. Figure 7.3 shows the spectrum of the predistorted input signal $\mathbf{x_d}$ at different values of the maximum polynomial order K. It's clear that the bandwidth increases as the maximum non-linear order K increases. This introduces demands to both the digital and analog electronics of the radar system. First of all, the sampling rate of the DAC must to be high enough to produce the IMD products without introducing aliasing, which effectively limits the maximum non-linear polynomial order of the behavioral models used for linearization. A signal with bandwidth 10 MHz will have a fifth-order IMD bandwidth of $5 * 10$ MHz $= 50$ MHz, which according to the Nyquist criterion requires 100 MHz to represent without aliasing. For the signal generator used for measurements in this thesis, the maximum sampling frequency is 100 MHz, meaning this limits the maximum non-linear order K for the models used for predistortion to $K = 5$ for a signal with 10 MHz bandwidth. For high bandwidth applications like the MIMO-OFDM radar in question in this thesis, this issue may be critical. These stringent demands to the

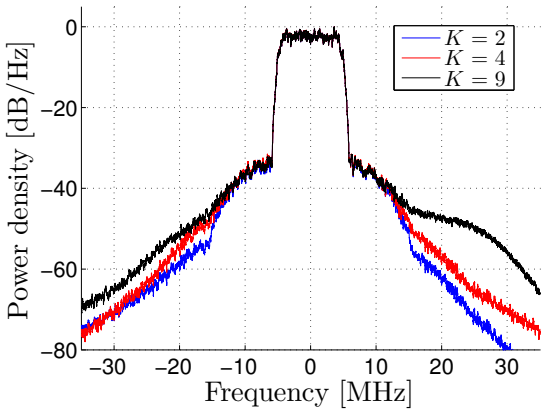

Figure 7.3: Power density spectra of predistorted 10W input signal $\mathbf{x_d}$ at different values of nonlinear order K.

DAC requires a trade-off between cost and linearization performance. The sampling rate of the DAC intended for transmission of the OFDM signal is 250 MHz. Predistortion will thus theoretically only be able to reduce spectral regrowth for the 50 MHz OFDM signal in a 125 MHz band. In addition, the increased bandwidth is important to consider when designing the analog electronics, as the IMD products have to be present until the signal has passed through the entire front-end system for the predistortion to work. If this has not been considered during the design of the radar system, it might prove costly to implement at later stages in the development process.

To see how critical this issue is, an additional set of measurements was performed on the 10W PA where a filter operation is applied on the predistorted input signal $\mathbf{x_d}$. Four Chebyshev filters $H_1, \cdots, H_4$, each with different "sharpness", are designed in MATLAB and used to filter $\mathbf{x_d}$ before transmission to the signal generator. The magnitude responses of the filters are shown in figure 7.4, together with the predistorted signal $\mathbf{x_d}$ spectrum.

This resulted in ACPR values shown in figure 7.5 which show that a filtering of the predistorted signal prior to the PA will definitely affect and potentially completely ruin the linearization. However the severity of this depends on the sharpness of the filter operation, as the less sharper filters still achieve some degree of ACPR reduction. From this it must be concluded that such filtering should be avoided, meaning the analog electronics at the DAC output must be able to handle the increased bandwidth of the predistorted signal.

A third concern is the increased PAPR of the predistorted signal. To compensate for gain compression, the predistorted input signal has higher peaks than the original input, meaning the DAC needs to be able to deliver enough power. A larger DAC is usually more power consuming, which might absorb the efficiency enhancement introduced by the predistortion operation. For this specific system, however, the most critical issue is not necessarily

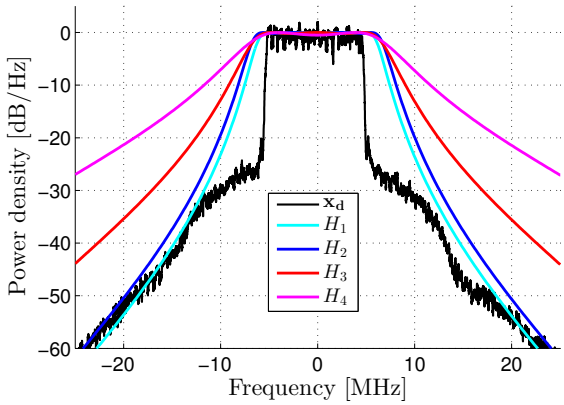

Figure 7.4: Power density spectrum for predistorted input $\mathbf{x_d}$ for 10W PA, $\bar{P}_{out} = 33$ dBm, and four filter magnitude responses.

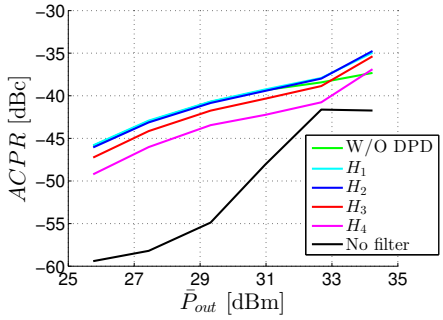

Figure 7.5: ACPR values for 10W OFDM signal predistorted with $MP_{4,3}^{all}$ model and filtered with four different filters before reaching the PA.

the total power consumption, but the power dissipation in the PA itself. Cooling of the system front-end is much more critical as the radar system consists of 64 separate radar channels each with an individual transmitter PA dissipating heat. Instead moving some of this power dissipation to the separately placed DAC might be advantageous.

7.5 Supplementary Comments

The purpose of this thesis was to show how digital predistortion linearization can benefit the MIMO-OFDM radar system. Linearization of the transmitter PA does have some benefits, however based on the results presented in this thesis they seem to be modest. After linearization, the ACPR of the OFDM signal was reduced by up to 10 dB for lower output powers, however this reduction was quickly consumed when output powers are increased.

For the radar system application, it's desirable to achieve high output powers, meaning digital predistortion will have limited benefits. A theoretical analysis performed in [25] shows the benefit of PA linearization in an OFDM system to be low, obtaining a maximum of 3 dB output back-off operating point improvement. This means that the PA could be driven 3 dB harder achieving the same linearity measured in EVM. The results presented in this thesis does not tell a vastly different story. Combining these results with the added complexity of adding a digital predistortion scheme, the costs might exceed the benefits of the implementation.

Chapter 8

Conclusion

8.1 Conclusion

The scope of this thesis was to investigate the linearization performance of digital predistortion of the Cree CMPA5585025F GaN PA intended as the transmitter PA in an X-band MIMO-OFDM radar system currently in development by the Norwegian Defence Research Establishment (FFI). This investigation was done by using mathematical behavioral models to linearize two RFPAs through digital predistortion. The first was a class F PA designed at NTNU based on the Cree 10W GaN transistor, and the second was the Cree CMPA5585025F GaN PA. By implementing indirect learning architecture algorithms in MATLAB based on the memoryless complex power series model, the Wiener model and the memory polynomial model, figures such as ACPR and EVM have been measured before and after linearization on 16-QAM and OFDM signals with 10 MHz bandwidth.

Modeling results showed that the MP model was superior in describing both PAs' behaviors, achieving an $NMSE(\mathbf{y}, \hat{\mathbf{y}})$ of -41 dB for the 10W PA, but only -22.5 dB for the 25W PA due to more severe memory effects which all models had a hard time representing.

The linearization results show that ACPR and EVM for a 16-QAM signal can be reduced by more than 15 dB and 5% respectively at the 1-dB compression point for the 10W PA using the $MP^{all}_{4,3}$ model. Only a more modest reduction was achieved for the 25W PA, with a reduction of 6 dB in ACPR and 3% in EVM at 1-dB compression, however the EVM results shows large variations and a confident conclusion regarding the EVM reduction can not be drawn. For the OFDM signal, ACPR was reduced by more than 15 dB for the 10W PA for lower power levels, however as power levels were increased, the reduction quickly worsened. For the 25W PA, ACPR reduction of the OFDM signal actually surpassed the reduction seen for the 16-QAM signal with a reduction of more than

10 dB using the $MP_{4,3}^{all}$ model, however this reduction was also quickly consumed as the output power was increased. The conclusion to draw from this is that there are not very clear benefits of implementing digital predistortion to the radar system. The additional cost of implementing the scheme and considerations regarding computational complexity and increased signal bandwidth may exceed the modest linearization benefits achieved in this thesis. The increased bandwidth issue was shown to be of great significance as a filtering of the predistorted signal prior to the power amplifier greatly reduced the linearization.

Integrating digital predistortion into the radar system may seem a trivial challenge from the outside, however it requires that both the digital and analog electronics have the necessary bandwidth to support the increased spectral bandwidth of the predistorted signal. If this has not been considered during the design of the radar system, it might prove costly to implement at this stage in the development process.

8.2 Further Work

In this thesis, the efficiency benefits of digital predistortion linearization only received a short superficial analysis. Further work should include a thorough efficiency analysis, to show how the power efficiency of the PA can be improved by allowing it to be driven harder before reaching the upper limit of distortion allowed. This could be of importance for the radar system as it consists of 64 individual radar channels which are closely spaced, making cooling a major challenge. The transmitter PA is the single biggest contributor to heat dissipation due to the high power outputs. Minimizing the heat dissipation in each channel will ease the issue of system cooling, making high efficiency desirable.

Due to the SMU200A vector signal generator's sampling rate of 100 MHz, the bandwidth of the OFDM signal was reduced from 50 MHz to 10 MHz in order to allow predistortion to be applied. In order to draw a more confident conclusion of the benefits of implementing DPD to the radar system, an analysis using a signal generator with a higher bandwidth should be performed. That said, the results presented in this thesis should give an indication of the benefits of such a DPD implementation, and that they in fact point toward limited benefits.

Bibliography

[1] Alasady et al. *Comparison Between Digital and Analog Predistortion for Satellite Communications*. IEEE, Canadian Conference on Electrical and Computer Engineering, 2003.

[2] Steve Cripps. *RF Power Amplifiers for Wireless Applications, 2nd ed.* Artech House, 2006.

[3] Steve Cripps. *Advanced Techniques in RF Power Amplifier Design*. Artech House, 2002.

[4] Schenk et al. *Frequency Synchronization for MIMO OFDM Wireless LAN Systems*. Vehicular Technology Conference, No. 58, 2010.

[5] Wu et al. *MIMO-OFDM Radar for Direction Estimation*. IET Radar, Sonar and Navigation, Vol. 4, Iss. 1, 2010.

[6] Lei et al. *The Sensitivity of Modulation Fidelity on PA Envelope Variation in OFDM Transmitter Systems*. EURASIP, Journal on Wireless Communications and Networking, No. 52, 2014.

[7] Andrea Goldsmith. *Wireless Communications*. Cambridge University Press, 2005.

[8] Rohde $ Schwarz. *Specifications, R& S SMU200A Vector Signal Generator, V. 08.00*, 2012.

[9] Kenneth G. Paterson. *On the Existence and Construction of Good Codes With Low Peak-to-Average Power Ratios*. IEEE, Transactions on Information Theory, Vol. 46, No. 6, 2000.

[10] S. Boyd and L. Vandenberghe. *Convex Optimization*. Cambridge University Press, 2004.

[11] Behzad Razavi. *RF Microelectronics, 2nd ed.* Pearson Education, 2011.

[12] Julian Christie Ertsås. *Digital Predistortion Methods for GaN Based RF Power Amplifiers*. Master's Thesis, Norwegian University of Science and Technology, 2012.

[13] J. Joh and J. del Alamo. *A Current-Transient Methodology for Trap Analysis for GaN High Electron Mobility Transistors*. IEEE, Transactions on Electron Devices, Vol. 58, 2011.

[14] David M. Pozar. *Microwave and RF Design of Wireless Systems*. John Wiley & Sons, Inc., 2000.

[15] Cree, Inc. *Technical Data Sheet, CGH40010F, Rev. 3.3*.

[16] Dragan Mitrevski. *Design and Characterization of a 6 W GaN HEMT Microwave Power Amplifier with Digital Predistortion Linearization*. Master's Thesis, Norwegian University of Science and Technology, 2011.

[17] Schreurs et al. *RF Power Amplifier Behavioral Modeling*. Cambridge University Press, 2009.

[18] Ye et al. *Linear and Nonlinear Memory Effects of RF Power Amplifiers*. IEEE, Asia-Pacific Microwave Conference, 2008.

[19] Raich et al. *On the Modeling of Memory Nonlinear Effects of Power Amplifiers for Communication Applications*. IEEE, Digital Signal Processing Workshop, 2002.

[20] Ding et al. *A Robust Digital Baseband Predistorter Constructed Using Memory Polynomials*. IEEE, Transactions on Signal Processing, Vol. 52, 2004.

[21] Morgan et al. *A Generalized Memory Polynomial Model for Digital Predistortion of RF Power Amplifiers*. IEEE, Transactions on Signal Processing, Vol. 54, 2006.

[22] J. Kim and K. Konstantinou. *Digital Predistortion of Wideband Signals Based on Power Amplifier Model With Memory*. IEEE, Electronic Letters, Vol. 37, No. 23, 2001.

[23] Martin Schetzen. *Theory of p-th Order Inverses of Nonlinear Systems*. IEEE, Transactions on Circuits and Systems, Vol Cas-23, No. 5, 1976.

[24] Cree Inc. *Technical Data Sheet, CMPA5585025F, Rev 3.2*.

[25] O'Droma et al. *Theoretical Analysis of Intermodulation Distortion in OFDM Signals in the Presence of Nonlinear RF High Power Amplifiers*. IEEE, Vehicular Technology Conference, No. 59, 2004.

Appendix A

PA Single-tone Characterizations

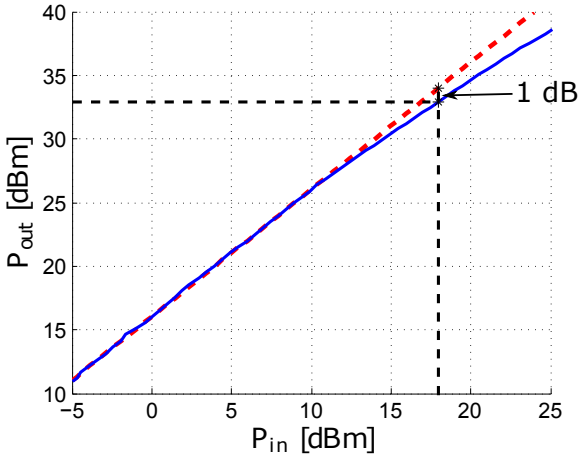

Figure A.1: Single-tone measurements on 10W PA, P_{out} as a function of P_{in} and P_{1dB}.

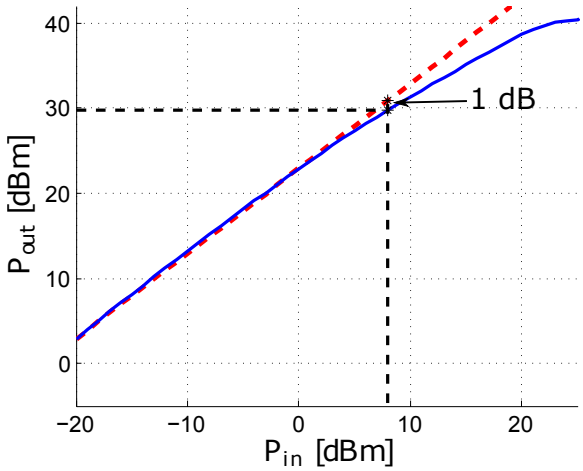

Figure A.2: Single-tone measurements on 25W PA, P_{out} as a function of P_{in} and P_{1dB}.

Appendix B

Selected MATLAB Code

B.1 Regression Matrix Generation

```
% ---- FUNCTION: GETMATRIX ---- %
%
% Author: Magnus Bache
%
% Function for generating regression matrix for the different
% behavoral models.
%
% Inputs:
% x -> PA input signal vector.
% y -> PA output signal vector.
% Model -> String specifying model.
% Orders -> String specifying polynomial orders.
% MaxOrder -> Maximum polynomial order.
% MemLength -> Memory length of model.
%
% Outputs:
% Hreg -> Regression matrix composed from input signal.

function Hreg = getMatrix(x,y,Model,Orders,MaxOrder,MemLength)

    if strcmpi('cps',Model)

        if (strcmpi('odd',Orders))
            Hreg = zeros(length(x),floor((MaxOrder+1)/2));
            for k = 1:floor((MaxOrder+1)/2)
                Hreg(:,k) = x.*abs(x.^(2*(k-1)));
            end
        elseif (strcmpi('even',Orders))
            Hreg = zeros(length(x),ceil((MaxOrder+1)/2));
            for k = 1:ceil((MaxOrder+1)/2)
```

```
            Hreg(:,k) = x.*abs(x.^(2*k-1));
        end
    elseif (strcmpi('all',Orders))
        Hreg = zeros(length(x),MaxOrder);
        for k = 1:MaxOrder
            Hreg(:,k) = x.*abs(x.^(k-1));
        end
    else
        error('Orders not specified correctly.');
    end

elseif strcmpi('mp',Model)

    lengthx = length(x);
    x = [zeros(MemLength,1); x];

    if (strcmpi('odd',Orders))
        Hreg = zeros(lengthx,MemLength*(floor((MaxOrder+1)/2)));
        for n = 1:lengthx
            for k = 1:floor((MaxOrder+1)/2)
                Hreg(n, (k-1)*MemLength + (1:MemLength)) = ...
                ((x((n+1):(n+MemLength))).*(abs(x((n+1):(n+MemLength)))...
                                        .^(2*(k-1)))).';
            end
        end
    elseif (strcmpi('even',Orders))
        Hreg = zeros(lengthx,MemLength*(ceil((MaxOrder+1)/2)));
        for n = 1:lengthx
            for k = 1:ceil((MaxOrder+1)/2)
                Hreg(n, (k-1)*MemLength + (1:MemLength)) = ...
                ((x((n+1):(n+MemLength))).*(abs(x((n+1):(n+MemLength)))...
                                        .^(2*k-1))).';
            end
        end
    elseif (strcmpi('all',Orders))
        Hreg = zeros(lengthx,MemLength*MaxOrder);
        for n = 1:lengthx
            for k = 1:MaxOrder
                Hreg(n, (k-1)*MemLength + (1:MemLength)) = ...
                ((x((n+1):(n+MemLength))).*(abs(x((n+1):(n+MemLength)))...
                                        .^(k-1))).';
            end
        end
    else
        error('Orders not specified correctly.');
    end

elseif strcmpi('w',Model)


    Hreg = zeros(length(x),MemLength);
    for m = 1:MemLength
        Hreg(:,m) = delay_signal(x,m);
    end
    if rank(Hreg)==min(size(Hreg))
        c1 = Hreg\y;
    else
```

```
        c1 = pinv((Hreg')*Hreg)*(Hreg')*y;
    end

    v = Hreg*c1;

    if (strcmpi('odd',Orders))
        Hreg = zeros(length(v),floor((MaxOrder+1)/2));
        for k = 1:floor((MaxOrder+1)/2)
            Hreg(:,k) = v.*abs(v.^(2*(k-1)));
        end
    elseif (strcmpi('even',Orders))
        Hreg = zeros(length(v),ceil((MaxOrder+1)/2));
        for k = 1:ceil((MaxOrder+1)/2)
            Hreg(:,k) = v.*abs(v.^(2*k-1));
        end
    elseif (strcmpi('all',Orders))
        Hreg = zeros(length(v),MaxOrder);
        for k = 1:MaxOrder
            Hreg(:,k) = v.*abs(v.^(k-1));
        end
    else
        error('Orders not specified correctly.');
    end

elseif strcmpi('h',Model)

    if (strcmpi('odd',Orders))
        Hreg = zeros(length(x),floor((MaxOrder+1)/2));
        for k = 1:floor((MaxOrder+1)/2)
            Hreg(:,k) = x.*abs(x.^(2*(k-1)));
        end
    elseif (strcmpi('even',Orders))
        Hreg = zeros(length(x),ceil((MaxOrder+1)/2));
        for k = 1:ceil((MaxOrder+1)/2)
            Hreg(:,k) = x.*abs(x.^(2*k-1));
        end
    elseif (strcmpi('all',Orders))
        Hreg = zeros(length(x),MaxOrder);
        for k = 1:MaxOrder
            Hreg(:,k) = x.*abs(x.^(k-1));
        end
    else
        error('Orders not specified correctly.');
    end
    if rank(Hreg)==min(size(Hreg))
        c1 = Hreg\y;
    else
        c1 = pinv((Hreg')*Hreg)*(Hreg')*y;
    end
    v = Hreg*c1;
    Hreg = zeros(length(v),MemLength);
    for m = 1:MemLength
        Hreg(:,m) = delay_signal(v,m);
    end

else
    error('Desired model is not possible.');
```

```
    end

end
```

B.2 Finding Coefficients and Model Output

```
% ---- FUNCTION: GETMODELANDOUTPUT ---- %
%
% Author: Magnus Bache
%
% Function for generating regression matrix for the different
% behavoral models.
%
% Inputs:
% x -> PA input signal vector.
% y -> PA output signal vector.
% Model -> String specifying model.
% Orders -> String specifying polynomial orders.
% MaxOrder -> Maximum polynomial order.
% MemLength -> Memory length of model.
%
% Outputs:
% y_hat -> Estimated model output.
% coeffs -> Vector with least-squares coefficients.
% Hreg -> Regression matrix composed from input signal.

function [y_hat,coeffs,Hreg] = getModelAndOutput(x,y,Model,Orders,MaxOrder,MemLength)

    Hreg = getMatrix(x,y,Model,Orders,MaxOrder,MemLength);

    if rank(Hreg)==min(size(Hreg));
        if strcmpi('mp',Model)
            lengthx = length(y);
            y = [zeros(MemLength,1); y];
            coeffs = Hreg\y(MemLength+(1:lengthx));
        else
            coeffs = Hreg\y;
        end

    else
        disp('Regression matrix rank deficient. Solving using pseudoinverse.');
        if strcmpi('mp',Model)
            lengthx = length(y);
            y = [zeros(MemLength,1); y];
            coeffs = pinv((Hreg')*Hreg)*(Hreg')*y(MemLength+(1:lengthx));
        else
            coeffs = pinv((Hreg')*Hreg)*(Hreg')*y;
        end
    end

    y_hat = Hreg*coeffs;

end
```

B.3 Script for Generation of Predistorted Signal

```
Pin = -16;                % Input power from generator [dBm];
Meas = 'DriverAndPA';     % Which data to use; ['Driver','DriverAndPA'].
What = 'FFI';             % Which amplifier; ['FFI','Richard'].
Signal = 'QAM';           % Which signal; ['QAM', 'OFDM'];

% ---- Model parameters ---- %

Model = 'mp';             % String specifying model; ['cps','mp','w','h'].
Orders = 'all';

% Memory length
MemLength = 3;            % Max memory length.
% Polynomial order
MaxOrder = 4;             % Max polynomial order.

% ---- Load file containing input and output data --- %

Path = 'C:/Users/.../';
fileName = sprintf('%s/Meas%s%s_%sPin%idBm.mat',Path,Meas,What,Signal,Pin);
load(fileName);

% ---- Find linear gain of PA ---- %

LinRegion = logical((abs(x)<0.4).*(abs(x)>0.05));  % Linear region of amplifier.
LinGain = mean(abs(y(LinRegion)./x(LinRegion)));  % Mean gain in linear region.

% ---- Find DPD coefficients ---- %

[~, DPDcoeffs] = getModelAndOutput(y/LinGain,x,Model,Orders,DPDOrder,DPDMemLength);

% --- Generate regression matrix ---- %

Hreg = getMatrix(x,y,Model,Orders,DPDOrder,DPDMemLength);

% ---- Generate predistorted signal ---- %

xDist = Hreg*DPDcoeffs;
```

B.4 Script for Sending And Receiving Data

```
clear all;
close all;
%% Set ports A and B

PORT1 = 1;
PORT2 = 2;

%% SG Parameters

RFpowdBm = 6;
```

```
RFfreqGHz = 2.0;            % in GHz
powLimdBm = 21;             % Limit for the peak input power
Pin = RFpowdBm;

%% SA Parameters
S.RefLevel_dBm = 30;
S.fs_Hz = fs;
S.RBW_MHz = 50; % SA Resolution BW when reading in IQ-mode
S.asr = 20e6;
Nper = 4; % nr of times the seq. is repeated
S.timebase = Nper * Nsamp / fs;
S.Npoints = ceil(Nper .* Nsamp .* S.asr ./ fs);

Meas = 'DriverAndPA';       % Which data to measure; ['Driver','DriverAndPA'].
What = 'Richard';
Signal = 'QAM';
% ---- Model parameters ---- %

%% Load input signal

fileName = sprintf('%s.mat',Signal);
load(fileName);

p2 = abs(x1).^2;
p = (p2 - min(p2)) / (max(p2) - min(p2));

% --- Calc. average RF power for the SG
PAPRdB = 10*log10(max(p) / mean(p));

if PAPRdB + RFpowdBm > powLimdBm
    error('Maximum input power exceeds POWLIMDBM.')
end

%% Load signal into SG
closecom
status = ConnectPortToIQOuput(PORT1);
SendWaveformTOSG_J(x1,RFfreqGHz,RFpowdBm,fs, PORT1); % Load RF-signal to the SG

% --- Get the I/Q data
[ySA, Settings] = CollectIQdata2(RFfreqGHz,2*Nsamp, S);
[ySAal, ynorm] = alignSignal(x1,ySA,128);

xNoDist = ynorm;
yNoDist = ySAal;

BW_channel = SR;
ACP_spacing = SR*(1+2*rolloff)*[1,2];
rolloffSA = rolloff;
[PodBm_nocomp, IM3and5dBcNoDist] = MeasACP_ALTP(RFfreqGHz*1e9,...
                                    BW_channel, ACP_spacing, rolloffSA);

fileName = sprintf('Meas%s%s_%sPin%idBm.mat',Meas,What,Signal,Pin);
save(fileName,'xNoDist','yNoDist','ovs','Nsym','filtdelay',...
            'rolloff','SR','fs','Nsamp','PodBm_nocomp','IM3and5dBcNoDist');
```